Numerical investigation of atmosphere-fire interactions during high-impact wildland fire events in Greece

Stergios Kartsios[a,*], Theodore Karacostas[a], Ioannis Pytharoulis[a], Alexandros P. Dimitrakopoulos[b]

[a] Department of Meteorology and Climatology, Faculty of Sciences, Aristotle University of Thessaloniki, Thessaloniki, Greece
[b] Laboratory of Forest Protection, Faculty of Agriculture, Forestry and Natural Environment, Aristotle University of Thessaloniki, Thessaloniki, Greece

ABSTRACT

This study investigated two high-impact wildland fire events that took place on 23 July 2018 in Attica Region, Central Greece during extreme prevailing weather conditions. The tragic aftermath was 102 life losses in MATI fire event, the largest number of deaths from a fire event in history of the country. The synoptic analysis revealed the presence of a positively tilted trough over the Central Mediterranean and Balkans, propagating eastwards and interacting with the subtropical jet, resulting in a strong westerly flow over Greece. Several surface stations in the wider area recorded wind gusts exceeding 20 m s^{-1} between 12:00 and 17:30 UTC. The online coupled atmosphere-fire model WRF-SFIRE was utilized in order to simulate these extreme fire events and to investigate the role of the complex terrain to the mean flow and fire behavior. The numerical simulations revealed the presence of induced orographic waves, paths of high winds on the lee-slopes, transient resemblance of a hydraulic jump downstream of Penteli Mt. (MATI), while indicated a downward transport of energy and momentum during the maximum wind speed occurrences. The turbulent and dynamically unstable conditions on the lee-slopes of Gerania Mts. (KINETA) and Penteli Mt. contributed to the flow kinetic energy. Quite different influences of topography in each fire event were found, where the isolated Gerania Mts. contributed to warmer, drier and windier conditions leeward, while Penteli Mt. had a lesser impact on atmospheric variables downstream.

1. Introduction

Extreme fire events are usually associated with atmospheric conditions at different spatial and temporal scales (Pereira et al., 2005) and are characterized by their duration (Amraoui et al., 2015), severity and the socioeconomic impact on the aftermath. Weather and climate define the favorable conditions in which these fire events may occur, affecting fuel properties such as fuel moisture and fuel accumulation.

The Mediterranean basin has experienced some of the most devastating fires in the last two decades, for example, the large fires of 2003 and 2005 in Portugal and of 2006 in Spain (Amraoui et al., 2013). The summer of 2007 was the worst year on record for forest fires in Greece, where extremely hot and dry weather conditions, combined with strong winds led to a disastrous upsurge of wildfires, evidence of a synergy of fuel and weather (Knorr et al., 2011; Koutsias et al., 2012).

The severity of fire events related to climate or weather extremes (Ahmad et al., 2019a, 2019b; Founda and Giannakopoulos, 2009; Powers et al., 2017; Tolika et al., 2009) from one hand and fuel accumulation and previous fire history (Minnich, 2001) from the other, has

been investigated (Keeley and Fotheringham, 2001; Minnich, 2001). Precipitation and evapotranspiration are strongly correlated with fire events, where these two variables affect the fuel load inflammability (Ahmad and Goparaju, 2019c). Under strong human pressure, the relationship between fire regimes and natural vegetation may be altered, even if the climatic conditions are not favorable for fire occurrence (Vázquez et al., 2002). According to Moriondo et al. (2006), climate change will increase the fire risk over the Mediterranean countries due to the increase in the number and the length of seasons with fire risk, but most importantly because of the increase of extreme events (e.g. longest dry spells, more frequent heat heaves).

Although the impact of topography into atmospheric flow and on the fire behavior have been described (Ahmad et al., 2018; Butler et al., 1998; Haines and Lyon, 1990; Rothermel, 1993; Sharples, 2009; Sharples et al., 2012; Simpson et al., 2013a, 2014, 2016), the role that mountain meteorological phenomena play in overall fire behavior is still an active field of research. Sharples (2009) provided a brief description of the key mountain meteorological phenomena that affect fire behavior (bushfires) such as, dynamic channeling, foehn winds,

low-level jets and mountain waves. Durran (1990) presented the fundamentals of the atmospheric motions occurring in a gravity wave forced by mountains (mountain wave) introducing downslope windstorms along the lee slope. Helmis et al. (2000) analyzed the results of an experimental study of downslope winds at Hymettus Mountain at Attica region, Greece and compared the observations with the Hydraulic-Like Theory (Long, 1953, 1955). Also, Koletsis et al. (2009) through numerical simulations showed that certain conditions such as the presence of a cross-barrier flow, a stable layer above mountain top and a critical level affected the wind speeds on the lee side during a wind event at northwest Greece. In literature, both observational and numerical studies (Clark and Peltier, 1984; Doyle and Durran, 2004; Doyle and Jiang, 2006; Durran and Klemp, 1987; Fudeyasu et al., 2008; Klemp and Lilly, 1975; Peltier and Clark, 1979; Sun, 2013) have been applied in order to investigate the flow structure of severe downslope winds associated with mountain waves. However, the linkage between mountain waves and fire behavior has been addressed to a smaller degree (Nauslar et al., 2018; Sharples et al., 2010; Simpson et al., 2013b).

In the Mediterranean region, past rural areas have turned into secondary homes, enlarging the wildland-urban interface (WUI). The majority of fire events is reported also there, while about 80% of the total burnt area in Europe concerns areas in this region. Among the natural, social and economic impacts, human casualties (civilians and firefighting crews) are the worst outcome in a fire event. During the period 1982–2007, the number of victims in Portugal and Spain was 110 and 186, respectively (Viegas, 2009), while in Greece 78 civilian lost their lives in the tragic events of the summer of 2007 (177 in total during 1980–2007). However, on 23 July 2018, the Greek nation faced another tragedy, where 102 civilians entrapped and lost their lives (directly or on the aftermath) due to extreme weather conditions, which led to aggressive fire behavior.

The first aim of this study is to present the two fire events (KINETA and MATI from now on) that took place on 23 July 2018 at Attica region in Greece and to analyze the prevailing weather conditions in the wider area (Fig. 1). The synoptic/mesoscale analysis revealed the presence of mountain waves. Thus, the second aim is to investigate the role of the complex terrain to the atmospheric flow, and how the latter affected the overall fire behavior.

In Section 2, the gridded analysis and observational data, the numerical model and the methodology employed are described. Section 3 presents the two fire events, the synoptic analysis and the weather conditions and investigates the existence of mountain waves in the airflow. In Section 4, the results of the numerical experiments are presented. Section 5 summarizes and concludes the findings of this study.

2. Data and numerical modelling system

For the purposes of this study, available surface observations, satellite imagery, data from the Copernicus Emergency Management Service - Mapping, global model analyses and very fine resolution model simulations were utilized. In addition, time series of available surface observations at Attica region (Fig. 1) were obtained from the Hellenic National Meteorological Service (HNMS). The record data consisted of 2 m air temperature and relative humidity, 10 min sustained wind speed and direction, wind gust speed at last 10 min and 3 h as well as daily precipitation, spanning from 22 (00Z) to 24 (12Z) July 2018, at 30 min intervals.

Panchromatic visible (0.4 to 1.1 μm) Meteosat SEVIRI images (0°E) from the NERC Satellite Receiving Station at Dundee University were examined, in order to distinguish key features of the synoptic flow and cloud formations. The burnt areas, in shape file format (.shp), were extracted from the Copernicus EMS (Emergency Management Service) – Mapping platform (event EMSR300, https://emergency.copernicus.eu/mapping/list-of-components/EMSR300, last accessed 28/06/2020),

while Sentinel-2A L1C images (True and False color) were used as additional information (only for the KINETA event). Moreover, the MODIS (Moderate Resolution Imaging Spectroradiometer) Fire and Thermal Anomalies product acquired from the Terra (MOD14) and Aqua (MYD14) satellites (Giglio et al., 2003) with spatial resolution of 1 km and the 375 m l-band data from the Visible Infrared Imaging Radiometer Suite (VIIRS) on Suomi NPP satellite (Schroeder et al., 2014) were retrieved for interpretation and validation purposes.

Synoptic analysis was carried out by employing the operational gridded analyses of the European Centre for Medium Range Weather Forecasts (ECMWF) at pressure levels, with 0.1° x 0.1° (latitude-longitude) grid spacing. At this grid resolution, synoptic and sub-synoptic scale features of the flow are resolved properly but certain flow characteristics (e.g. mountain waves) with wavelengths smaller than ~9 km are not captured.

The numerical modelling system WRF-SFIRE (Mandel et al., 2011, 2014) was adopted in order to simulate the two fire events under high fire weather severity. The version 3.4.1 of the WRF-ARW model (Wang et al., 2012) was utilized as the available release in the WRF-SFIRE distribution. WRF-SFIRE has been positively evaluated and implemented both in real and idealized cases (Dobrinkova et al., 2011; Farguell et al., 2017; Giannaros et al., 2019; Jordanov et al., 2012; José et al., 2014; Kartsios et al., 2014a, 2014b, 2017; Kochanski et al., 2013a, 2013b, 2013c, 2016; Koletsis et al., 2016; Lagouvardos et al., 2019; Peace et al., 2016; Simpson et al., 2013a, 2014, 2016).

The domain setup (Fig. 2a) consisted of three, 2-way telescoping nests, which covered parts of Southeast Italy, South Balkans, Greece and West Turkey (d01, 308 × 239 × 39 grid points), Central Greece and Peloponnese (d02, 259 × 193 × 39 grid points) and Attica region (d03, 283 × 205 × 39 grid points), with horizontal grid spacings of 5 km, 1.67 km and 0.55 km, respectively. In vertical, 39 sigma levels, up to 50 hPa were manually defined, with increased resolution in the boundary layer. The first theta level was located at approximately 10 m above terrain height. The fire module was activated in the innermost domain (d03), where the surface fire mesh had a refinement ratio 1:20, which corresponds to 27.77 m horizontal fire-grid cell size. Initial and boundary conditions for the outer domain were extracted from the ECMWF operational analyses (0.1° x 0.1° lat.-long.), at 6-hourly intervals. Model initialization was placed at 00Z on 23rd of July 2018, almost 9 h prior to the fire ignition at Gerania Mts. (KINETA event), while the simulation time window was 36 h. Model output was available every 5 min, at hourly intervals and every 3 h for the finer (d03), the intermediate (d02) and the coarser (d01) domain, respectively. The first 6 simulated hours were considered as model "spin-up" and were not included into the analysis. The spin-up time is of paramount importance for the model to derive a valid physical state (Ulmer and Balss, 2016) and this time interval considered in several numerical modelling studies (e.g. Koletsis et al., 2016; Matsangouras et al., 2016; Pytharoulis, 2018; Pytharoulis et al., 2016, 2018; Weiss et al., 2008; Yair et al., 2010).

The wind field from the atmospheric model has been inserted to the spread rate formula by first vertically interpolating to common height (6.096 m), using the roughness length values from land use and then multiplying by prescribed wind reduction factors (Baughman and Albini, 1980; Mandel et al., 2011). Although a number of options, which control the process of the wind digestion to the fire model, are available, the aforementioned choice was based on its simplicity and computational efficiency. The heat fluxes from the fire are assumed to exponentially decrease with height through the heat extinction depth formulation. As the 1st theta model level was placed at approximately 10 m above ground level (agl), the default value of 50 m was used as e-folding depth. The role of the latter to the fire behavior was investigated in Kartsios et al. (2017). Also, the fuel-moisture model (Mandel et al., 2014) was activated, allowing proper responses between fuel moisture and atmospheric conditions, while fire emissions were available as passive tracers (smoke).

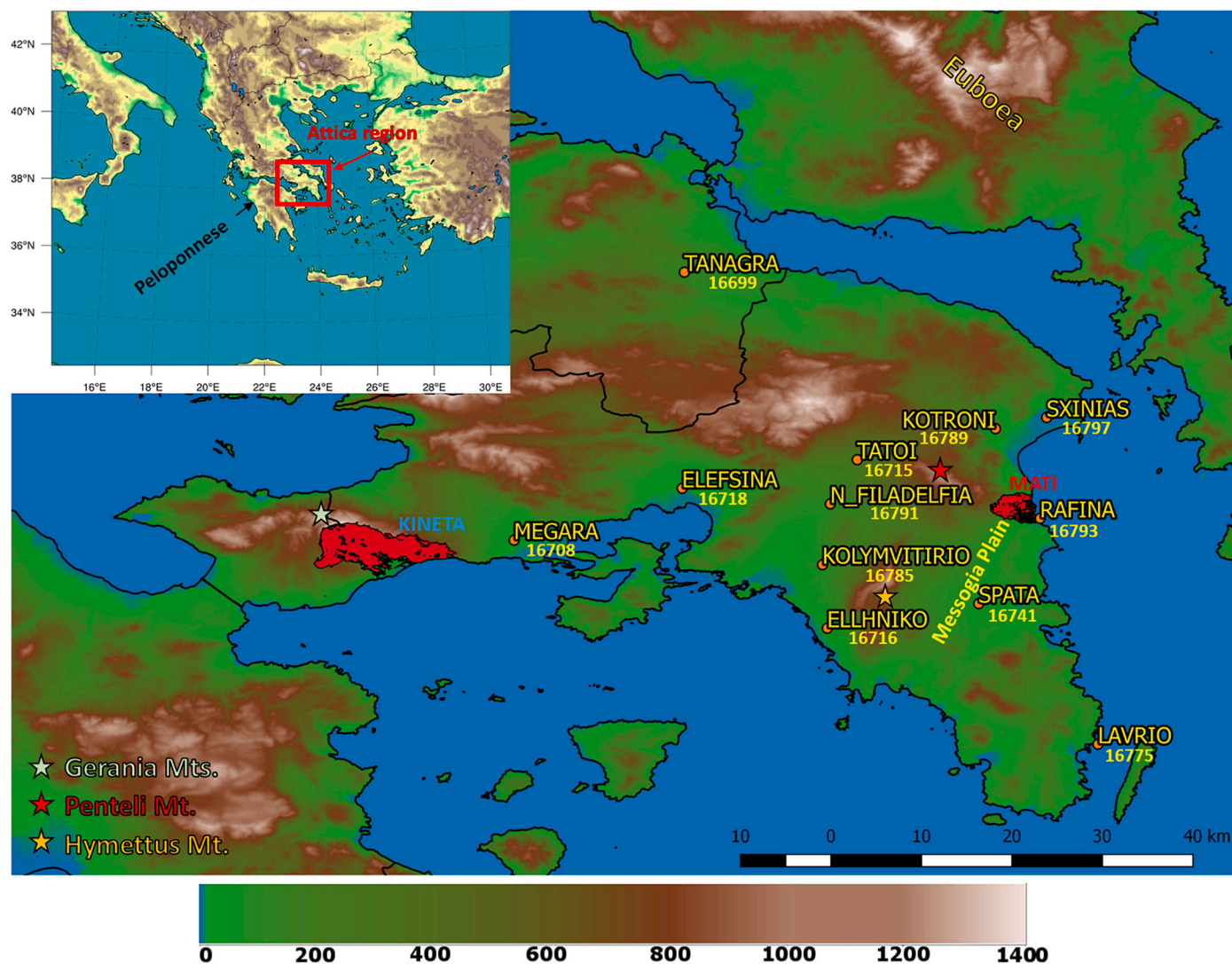Land use representation was based on CORINE Land Cover (CLC)

Fig. 1. The wider area of Attica Region, Greece and its topography (m, shaded contours). The observed burnt areas of KINETA and MATI fire events (red scars) are illustrated along with the locations of HNMS surface observations (including their World Meteorological Organization identification numbers).

2006 data (100 m × 100 m) mapped and interpolated to the 1 km-resolution International Geosphere-Biosphere Programme (IGBP)-MODIS vegetation classification. Moreover, a soil texture map for Europe at 1 km based on the HWSD (Harmonized World Soil Database) v1.2 was inserted to the model as additional information (Josipa et al., 2014). The SFIRE demands very fine spatial resolution topographical and fuel data, in order to represent accurately the sub-grid variability in topography and fuel composition. Thus, the Shuttle Radar Topography Mission data (SRTM v3, 30 m × 30 m, 1 arc-*sec*, Farr et al., 2007; NASA, 2013) were retrieved, properly converted and digested into the innermost domain (d03) and the fire model. The horizontal resolution of the SRTM dataset is approximately equal to the fire-grid discretization, ensuring properly calculated slope gradients (Mandel et al., 2011). Description of the available fuels at Attica region (d03) was achieved by reclassifying CORINE 2012 raster data (v18, 100 m × 100 m) into fuel models according to the Northern Forest Fire Laboratory (NFFL) classification (Anderson, 1982) and resampling them (nearest neighbor) into 30 m × 30 m spatial resolution (Fig. 2b). Lacking any finer re-solution fuel dataset, publicly available for Greece and already con-verted into NFFL fuel models as well, the conversion matrix (Table 1) was based on literature regarding Mediterranean ecosystems (Benali et al., 2016; Duguy et al., 2007; Jordanov et al., 2012; Kalabokidis et al., 2012; Sá et al., 2017; Sebastián López et al., 2002). Each NFFL

fuel category (13 in total) is associated with specific fuel properties, such as fuel density, depth and mass, surface to volume ratio, mineral content and moisture of extinction, which are provided externally to the fire module. Although these fuel properties were based on field work in the United States, no any adjustments were considered. In addition, in the wildland-urban interface (WUI) of the devastating MATI fire event, the fuel type based on CORINE 2012 would be originally translated as non-burnable (NFFL fuel type 14; Table 1). Therefore, the corre-sponding grid-points were manually assigned into NFFL fuel type 6 (Dormant brush, hardwood slash), based on subjective observational analysis of the area and numerical sensitivity experiments (e.g. with NFFL fuel type 2, Timber).

The parameterization of microphysical processes was carried out by the Eta-Ferrier scheme (ETA; Rogers et al., 2001). The RRTMG scheme (Iacono et al., 2008) was used, for the shortwave and longwave ra-diation, with the slope effects option active in order to modify the surface solar radiation flux according to terrain slope. Boundary layer processes were represented by the Mellor-Yamada-Janjic scheme (MYJ; Janjić, 1994, 2002), surface layer by the Eta similarity scheme (Monin and Obukhov, 1954; Janjić, 1994, 1996, 2002), based on Monin-Obu-khov with Zilitinkevich thermal roughness length, while the soil properties and land-atmosphere interactions were described by the Unified Noah Land Surface Model (NOAH; Chen and Dudhia, 2002;
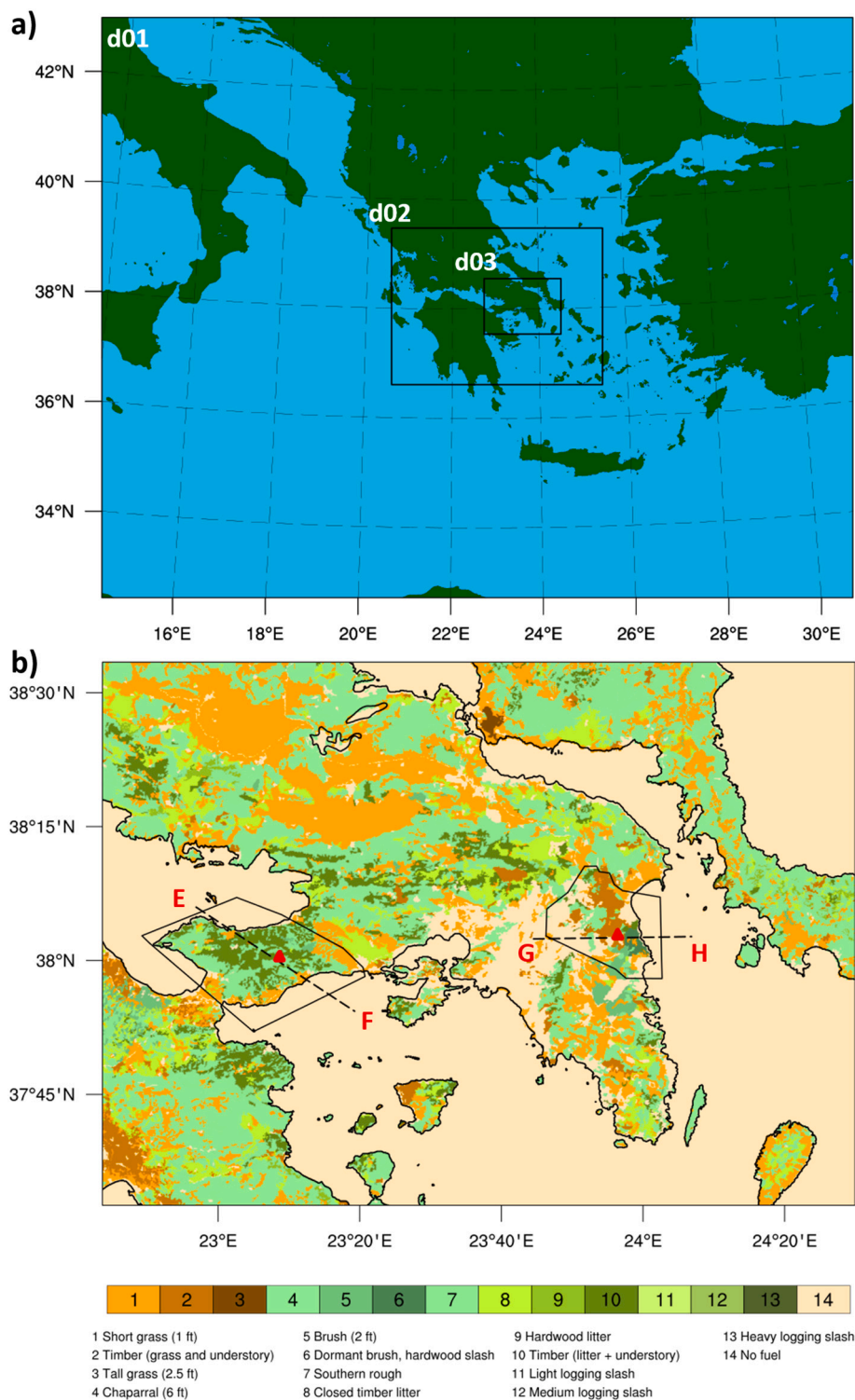
Fig. 2. a) Domain configuration and b) the innermost domain (d03) extent with NFFL fuel spatial distribution (shaded) and actual fire ignition points (red triangles) at KINETA and MATI events. The dashed lines indicate the locations of the cross-sections in Fig. 8. The black solid polygons encompass the areas in which the topography was removed in the sensitivity experiments of sub-section 4.3.

Tewari et al., 2004). The Betts–Miller–Janjic scheme (BMJ; Janjić, 1994, 2002,) was responsible for the parameterization of sub-grid convection. The convection scheme was activated only in the outer nest (d01), following other numerical studies in the wider Mediterranean region (Karacostas et al., 2018; Kotroni and Lagouvardos, 2004; Lagouvardos et al., 2013; Pytharoulis et al., 2016; Sindosi et al., 2012). The model physics configuration was consistent in all three domains,

while it has been tested and used during the operational period (2013–2015) of Wave4Us (Wave climate and coastal circulation Forecasts for public Use; http://wave4us.web.auth.gr) project in Greece. Although the domain configuration was different in the operational model, this physics suite has been verified and found to be in good agreement with the observations (Pytharoulis et al., 2015; Krestenitis et al., 2017).

Table 1
Conversion matrix of CLC 2012 land uses to NFFL fuel models (Anderson, 1982).

CORINE land cover code	NFFL fuel model	Description
111, 112, 121, 122, 123, 124, 131, 132, 133, 213, 331, 332, 335, 421, 422, 423, 511, 512, 521, 522, 523	14	No fuel
142, 211, 212, 231, 242, 321, 411	1	Short grasses (30 cm)
141, 222, 244, 333	2	Timber (grass and understory)
241	3	Tall grass (76 cm)
323	4	Chaparral (183 cm)
221, 412	5	Brush (61 cm)
322	6	Dormant brush, hardwood slash
243, 324	7	Southern rough
223, 313, 334	8	Closed timber litter
311	9	Hardwood litter
312	10	Timber (litter and understory)

3. Synoptic and mesoscale analysis

3.1. Description of the events

On 23rd of July 2018, two wildfires broke out at Attica region (Central Greece), under strong westerly - northwesterly flow, high temperatures and low values of relative humidity. According to the National Observatory of Athens (NOA), wind gusts exceeded 27 m s^{-1} at several sites of Attica that day. At approximately 09:03 UTC (12:03 LT), a wildfire was reported in Gerania Mts., at "Aeras" location (KINETA; Fig. 1, Fig. 2b), northwest of Kineta settlement, at the regional unit of West Attica. The wider area is part of the European Network of Protected Areas – Natura 2000 (http://ec.europa.eu/environment/nature/natura2000/ data/index_en.htm). The local settlements were evacuated, but despite the efforts of the Fire Service, the fire was active until the late hours of the 25th of July 2018, totally burning two settlements and partially another one.

Nearly 4.5 h later, at 13:49 UTC (16:49 LT) on 23July 2018, a fire-spot was reported at Kallitehnoupolis settlement (Ntaou) on Penteli Mt. (Municipality of Rafina), at East Attica regional unit (MATI; Fig. 1, Fig. 2b). Unofficial reports (e.g. video footage) placed the fire ignition time 8 min prior to the officially reported time (13:49 UTC), while the Automated Weather Station (AWS) in Penteli Mt. (close to the ignition point of the MATI fire event; Fig. 1, Fig. 2b) recorded gusts reaching 25 m s^{-1} between 1230 and 1430 UTC (Lagouvardos et al., 2019). It quickly became evident that the air forces were unable to operate due to the strong wind field. Under such extreme windy conditions, the fire spread fast towards east through several settlements, where it finally stopped at the coastal area of Mati in less than 2 h (Fig. 1). In addition, the fuel type (mostly Mediterranean pine species such as *Pinus halepensis*) and fuel loading of the area, assisted the intensification of the event. Dimitrakopoulos and Panov (2001) quantified the chemical and physical properties of several dominant species in the eastern Mediterranean Basin. They found that *Pinus halepensis* presents high mean values of surface area-to-volume ratio (leaves, 62.49 cm^{-1}) and relatively low mean particle density (leaves, 0.29 g m^{-3}), thus high heat and moisture exchange rates (Brown, 1970) and lower thermal conductivity, meaning faster ignition times (Anderson, 1970), respectively. The aforementioned, in conjunction with the special morphology of the area (wildland-urban interface) and the narrow streets resulted to minimal response times by the inhabitants and the local authorities. The tragic aftermath was 102 loss of lives (the majority of them were entrapped by the fire), several settlements were burnt, over 1500 structures and vehicles were burnt or damaged, while parts of electricity, water supply and telecommunication networks were greatly affected. According to the Hellenic Fire Service, the fire was totally suppressed the next day (24th of July 2018).

3.2. Synoptic analysis

The prevailing synoptic conditions, which greatly influenced the behavior and evolution of the two extreme fire events in the Attica region on 23July 2018, are presented along with the available surface observations.

According to the ECMWF operational analyses on 23/07 00Z, at 500 hPa, a low upper air system was dominating north and east of the Greek region, while a southwest-northeast (positively tilted) oriented short wave trough had been developed west of North Italy, over Sardinia. Moreover, a high upper air system was located over Atlas Mountains in North Africa, at 500 hPa, with its eastern flank elongating southwest of Greece. As a result, a west-northwest flow was prevailing over the area of interest (Fig. 3a). This synoptic pattern was coherent in the vertical, resembling the zonal flow circulation type, according to Karacostas et al. (1992) and Karacostas (2003) synoptic classification. Also, the position of the subtropical jet stream coincided with the mid-tropospheric baroclinic zone, where wind speeds stronger than 55 m s^{-1} were present into its core (Fig. 3a). The area of interest is located very close to the right flank of the jet stream exit, which is associated with subsidence. In the following hours, the short wave trough moved eastwards and merged with the low upper air system resulting in a closed long wave trough with no significant deepening of the isoheights (contours), while the position of the upper air ridge remained almost unchanged (Fig. 3b). Examination of the potential temperature field at 850 hPa (Fig. 3c) revealed an eastwards cold air advection (CAA) over the Greek area (23/07, 12Z), which produced isentropic downglide and sinking. The west-northwest flow is also evident, while the wind speed at that level exceeded 40 knots (≈ 20 m s^{-1}) over the central and southern Greece. According to the Met Office surface analysis chart at 12Z on 23/07 (not shown), an upper tropospheric cold front was present (Fig. 3b), moved southeastwards and dissipated in the following hours, influencing the area of interest (Attica region). In addition, on 23/07 at 12Z, a relatively weak southwest–northeast mean sea-level pressure (MSLP) gradient (Fig. 3d) force was present. Moreover, a 2 m air temperature gradient between western and eastern Greece (23/07, 12Z) was developed (Fig. 3d), where the temperature lied above 36 °C over the eastern parts and the 2 m relative humidity dropped below 20% (not shown) according to ECMWF analyses.

The examination of HNMS surface observations (Fig. 1) revealed that, windy conditions persisted from 07Z until 22Z on 23 July 2018. The maximum wind speed (gust) was 16.6 (23.6) m s^{-1} at Elefsina (16718; Fig. S1a), 8.4 (15.3) m s^{-1} at Ellhniko airport (16716; Fig. S1b), 9.3 (15.9) m s^{-1} at Tatoi (16715; Fig. S1c) and 11.8 (25.2) m s^{-1} at Rafina station (16793; Fig. S1d). For the same period, Elefsina (Fig. S1a), Ellhniko (Fig. S1b) and Tatoi (Fig. S1c) experienced lower maximum temperatures (37.4 °C, 34.8 °C, 36.0 °C, respectively) than Rafina (39 °C) (Fig. S1d). In addition, the maximum temperature at Ellhniko was 3 °C higher than the climatological mean for July (31.8 °C), while at Tatoi, the difference was 3.9 °C (mean max. 32.1 °C) according to HNMS. Moreover, at Rafina station (Fig. S1d), a rapid increase on temperature values was observed between 09Z and 11Z with simultaneously decrease in dew point temperature and relative humidity below 15%, resulting in increased potentiality for extreme fire behavior
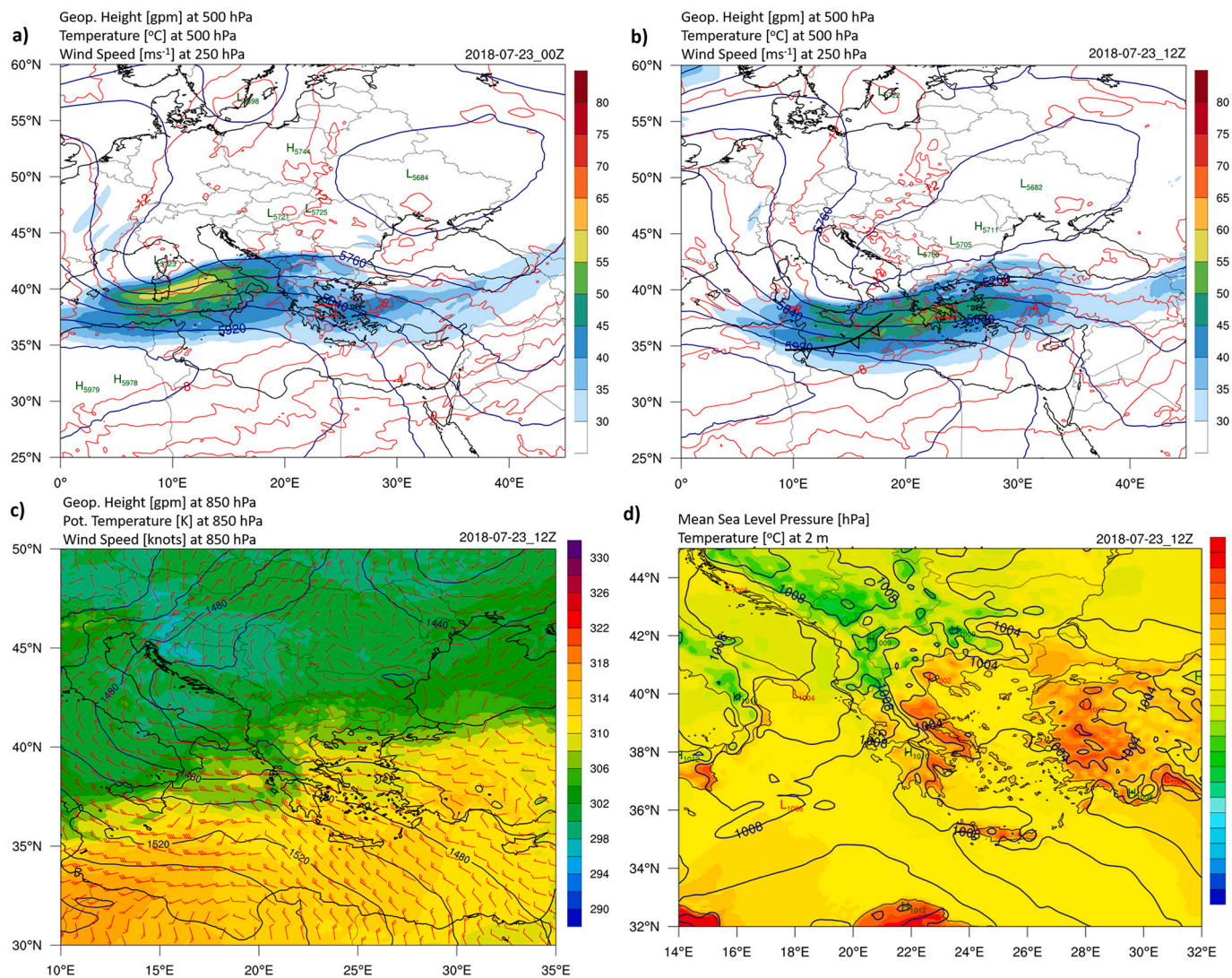
Fig. 3. a,b) Horizontal sections of geopotential height (gpm, blue contours) and temperature (°C, red contours) at 500 hPa, wind speed (m s^{-1}, shaded contours), at 00:00 UTC and 12:00 UTC, on 23 July 2018, respectively, c) geopotential height (gpm, contours), potential temperature (K, shaded contours), wind speed and direction (knots, windbards, half barb = 5 knots, full barb = 10 knots) at 850 hPa and d) mean sea-level pressure (hPa, contours) and 2 m air temperature (°C, shaded contours), at 12:00 UTC, on 23 July 2018, according to the operational ECMWF analyses. In panels (a) and (b) the red rectangle encompasses the greater area of interest (Attica), while in panel (b), the location of an upper air cold front has been reproduced from the corresponding UK Met Office surface analysis chart.

(Sharples, 2009; Sharples et al., 2010). At the same time, a nearly 180° change in wind direction is evident there (transition from sea breeze conditions to synoptic forcing) and was not related with the passage of the upper cold front that was depicted on (Fig. 3b). According to the analyses, the cold front influenced the area of interest a few hours later (between 12Z and 18Z). The increased wind speed and gust records along with the approximately westerly flow were observed at all available HNMS stations (not shown), due to the previously presented synoptic forcing.

The calculated Fosberg Fire Weather Index (FFWI) (Fosberg, 1983) presented medium to high fire weather severity almost at all HNMS stations of Attica Region (Fig. S2), while at Elefsina and Kotroni sites, the FFWI escalated rapidly to very high values, at specific time windows since 12Z (max. 74.15 and 74.13, respectively). At Megara, which is the closest available observational HNMS station to KINETA event, fire risk was estimated as high from 14Z and afterwards (max. 52.4). Moreover, variations in FFWI level are observed at Rafina until 12:30 UTC, while at the time of the fire ignition (13:49 UTC) at Kallitehnopoulis settlement (MATI event), the fire risk was high (max. 57.1). FFWI presents stronger dependency on wind speed and relative humidity rather than

temperature (Roads et al., 1991). Under windy, dry and relative warm conditions, higher FFWI values are expected. The latter could explain why at Rafina, lowest values of FFWI were presented despite the higher observed temperatures in comparison to other sites, such as Elefsina and Kotroni. However, the FFWI was able to represent the temporal variation of fire weather severity at all sites with available data.

3.3. Airflow modification

The moderate background westerly flow led to local airflow modification (Barry, 1992; Whiteman, 2000) due to the presence of topographic barriers. Under certain conditions, the presence of mountain waves over the wider area of Attica resulted to the development of strong katabatic winds at the lee side of any barrier perpendicularly oriented to the flow in the region (Helmis et al., 2000).

Fig. 4a depicts longitude – pressure section of potential temperature (K) and u-wind component (m s^{-1}) at 38°N on 23/07 at 06Z, prior to the KINETA fire ignition, according to the ECMWF operational analyses. Locations of the KINETA and MATI fire events leeward of Gerania Mts. and Penteli Mt. are marked with black and red short lines,
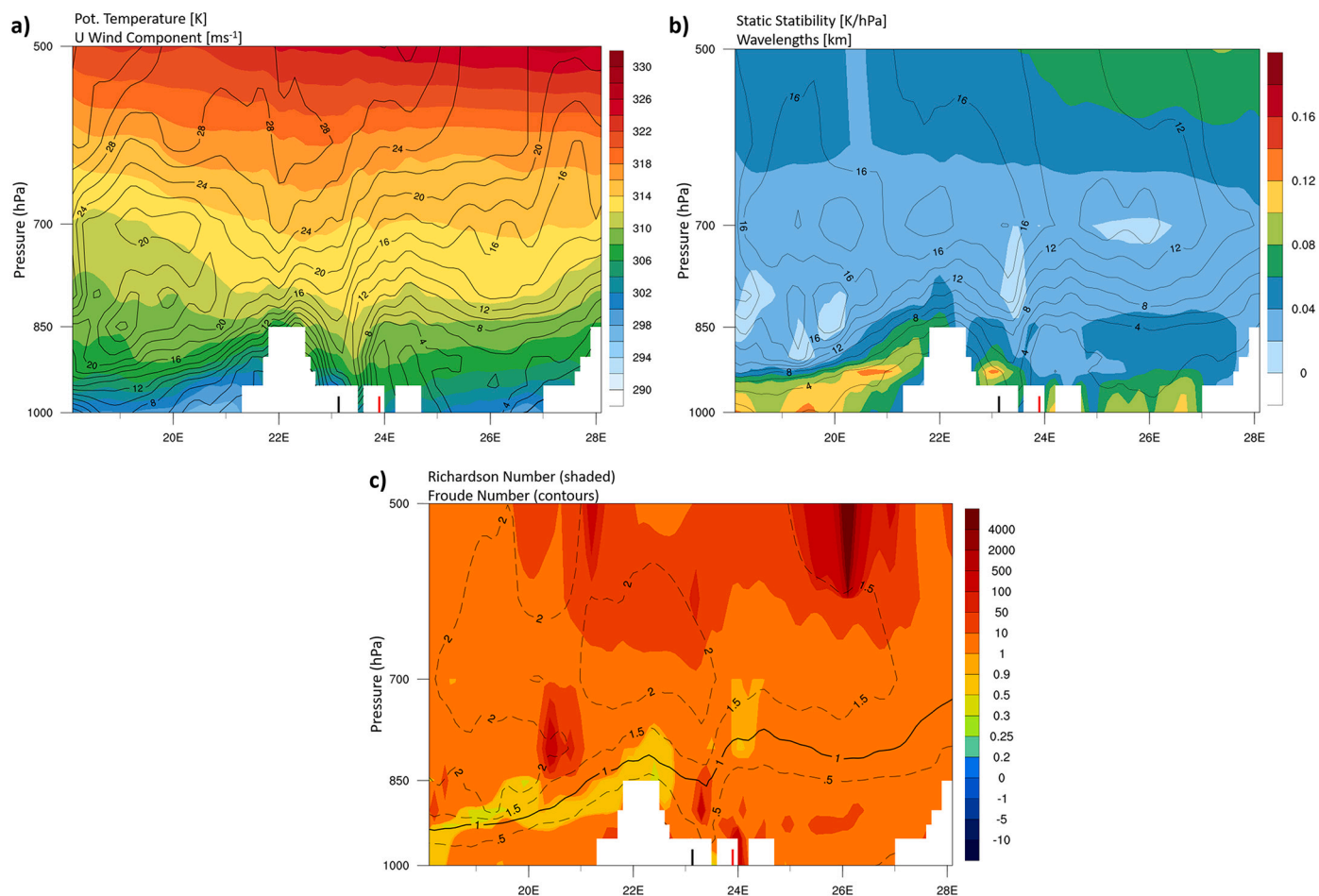
Fig. 4. Longitude – pressure section of a) potential temperature (K, shaded contours) and u-wind component (m s^{-1}, contours), b) static stability (K hPa^{-1}, shaded contours) and wavelengths (km, contours) and c) Richardson (shaded contours) and Froude (contours) numbers, at 38°N on 23/07 at 06Z (ECMWF operational analyses). Black and red line marks indicate the locations of Gerania Mts. and Penteli Mt., respectively.

respectively. The fast isentropic lifting windward and descent downwind of Gerania Mts. (black line mark), along with the upwind deceleration of the flow and the rapid increase of the u-wind speed at the lee side (downwind jump), declares the presence of induced orographic waves (Fudeyasu et al., 2008). As a result, warm air advection from lower to higher layers is occurring while at the same time dry and cold air descents lower (Theta-E contours, not shown). Due to lifting of moist layers (Theta-E contours, not shown), clouds are expected, which is in agreement with the observed cloud formations from the satellite images (not shown).

From 22°E to 24°E, the isentopes are nearly vertical at specific regions near the surface implying near-adiabatic conditions and almost neutral static stability (Bluestein, 1992; Young, 2003), which ranges from 0.02 to 0.06 K hPa^{-1} (Fig. 4b). Moreover, two regions of increased stability (Fig. 4b) are observed. A wide area from 18°E to 22°E, with maximum values at 900 hPa and aloft of Gerania Mts. (0.13 K hPa^{-1}) at the same isobaric level, implying faster oscillations (e.g. larger Brunt-Väisälä frequencies), maximum displacements of the air parcels and fast horizontal wave speeds (Young, 2003). The former area covers the northern part of Peloponnese (Fig. 1), where complex terrain is present across the section. Downwind of the Penteli Mt. (red line mark) and eastwards, the lower troposphere is also subjected to vertical displacements, however to a lesser degree, mostly due to the presence of the southern part of Euboea. In addition, calculated wavelengths (λ), $2\pi/l(z)$ (l(z) is the Scorer parameter, (Barry, 1992; Scorer and Klieforth, 1959)), of the potential formed waves are presented in Fig. 4b. Their magnitude allowed for possible interaction of their descending parts

with the lee side of the orographic barriers in the area of interest, where λ < 4 km.

The formation of waves is supported by the values of Froude number (Fig. 4c, contours), which are below but close to unity up to 850 hPa (Smolarkiewicz and Rotunno, 1989; Stull, 1994). The vertical tilting of the 0.5 contour line between Gerania Mts. and Penteli Mt., is also worth noticing, since the formulation of the Froude number is a function of wind speed across the mountain. The gradient Richardson number (Stull, 1994), Ri, (Fig. 4c, shaded contours) lies between 0.3 and 1, along the solid contour line (critical value equal to unity) of Froude's number and in a limited area around Gerania Mts., closed to the surface. This implies that possibly the flow was dynamically unstable and turbulent (due to shear production) at these regions, although Richardson number never gets values below critical (Ri$_c$ = 0.25). However, in the following hours the Ri became smaller than 0.25 close to the surface and in the area of interest (Gerania Mts – Penteli Mt.) with the Froude number equals to unity at the same time (not shown).

The ECMWF analyses represented the magnitude of wind speed, temperature and relative humidity variations to some degree upon the area of interest but failed to capture the embedded variability mostly due to relatively coarse temporal and spatial resolution. To shed light upon the mechanisms that produced such windy conditions over the Attica region and affected the overall fire behavior at KINETA and MATI fire events, high spatiotemporal resolution numerical simulations were utilized. In the next section, the role of topography into the prevailing weather conditions on 23 July 2018 is investigated, along with

the simulated fire behavior in both events.

4. Numerical simulations

The meteorological conditions along with the two extreme fire events on 23 July 2018 were simulated by utilizing the WRF-SFIRE modelling system. In total, four (4) experiments, with very high spatial and temporal resolution were performed in order to address the role of topography into the development of mountain waves and the associated fire behavior in each event. The control experiment (CNTRL) was based on the model configuration described in Section 2. In TOPOG and TOPOP experiments, the topography of Gerania Mts. (KINETA) and Penteli Mt. (MATI) (black solid polygon lines, Fig. 2b) was removed, by setting the corresponding grid points equal to zero in all domains, respectively. Moreover, a three (3) grid point smoothing was applied at the borders of each area, in order to avoid numerical instabilities due to the produced steep slopes. In NTOPO experiment, the topography of the innermost domain (d03) was completely removed in all nests, following the methodology in Pytharoulis et al. (2016). At all sensitivity experiments (TOPOG, TOPOP, NTOPO) the model configuration remained the same as in the CNTRL experiment.

4.1. Model verification

Statistical evaluation was carried out in the CNTRL experiment at the innermost (d03) domain, using all the available HNMS surface observations (12 stations). The first six (6) hours were not accounted in the results (spin-up) and the model verification was performed from 06:00 UTC on 23 July 2018 to 12:00 UTC, on 24 July 2018.

Each forecast value was obtained by first finding the four (4) grid points closest to the location of the observation and then applying the Inverse Distance Weighting (IDW) interpolation method (Isaaks and Srivastava, 1989; Li and Heap, 2014). The model grid points over the sea were filtered from the calculations.

The model was verified in terms of 2 m air temperature (Tmp), 2 m relative humidity (Rh) and 10 m wind speed (Wspd) for all the pairs of forecast versus observed values. The model errors with their corresponding confidence intervals at 95% significance level are illustrated in Table 2. The calculated errors were first averaged spatially and then temporally. The model overestimated Tmp and Wspd by 1.4 ± 0.2 K and 1.9 ± 0.3 m s^{-1}, while the ME in Rh was underestimated ($-3.7 \pm 1.0\%$). The MAE (RMSE) of Tmp, Rh and Wspd were found equal to 1.8 ± 0.1 (2.2 ± 0.8) K, 8.7 ± 0.7 (11.6 ± 5.0) % and 2.8 ± 0.2 (3.6 ± 1.3) m s^{-1}, respectively. Moreover, the simulated and observed temperature values were highly correlated (Pearson, 0.92, $p = 0.01$), while for the relative humidity and wind speed, the corresponding Pearson correlation coefficients were found equal to 0.75 and 0.56 ($p = 0.01$). In addition, the standard deviation for the Tmp, Rh and Wspd MAEs was 1.3 K, 7.7% and 2.2 m s^{-1}, respectively. The above scores align with previous studies of the intense meteorological events and operational weather forecasting in the wider area of Mediterranean and Greece (Koletsis et al., 2016; Kotroni et al., 2014; Krestenitis et al., 2017; Matsangouras et al., 2014, 2016; Papadopoulos and Katsafados, 2009; Pytharoulis et al., 2015, 2016), revealing an overall satisfactory model performance.

Regarding the temporal evolution of the ME and MAE, the model presented the largest absolute errors in Tmp variable during the warm hours (23/07 10:00–16:00 UTC, 24/07 06:00–10:00 UTC), when Tmp was overestimated (Fig. S3a). The overestimation in Tmp from T + 10 to T + 16 (23/07 10:00–16:00 UTC) coincided with the largest errors in Wspd (Fig. S3c) and the onset of the fire events at KINETA and MATI areas. The MAE of Rh was nearly constant during the simulation (Fig. S3b), while a clear underestimation was shown from T + 23 h (23/07 23:00 UTC) and onwards, which was associated with a gradual 180 degrees change in wind direction and moisture advection in the model.

4.2. Control experiment (CNTRL)

4.2.1. Simulated atmospheric conditions

The online coupled model was able to capture the temporal evolution of the prevailing meteorological variables at surface and the onset of the windy conditions to a certain degree, but showed discrepancies in temperature and wind speed maximum values (both in time and magnitude) in comparison to the observational data. However, regarding the wind speed field, recorded wind gusts from the HNMS stations are on the same magnitude as the simulated wind speed (e.g. Tatoi: obs = 15.9 m s^{-1}, model = 15.0 m s^{-1}). It must be considered that at each model output, the simulated wind speed was close to the temporal variation of the gusts than the observed 10 min sustained wind speed from the HNMS data, which may justify the aforementioned differences. Also, one must not neglect the uncertainty on the observational data (Haylock et al., 2008; Klein Tank et al., 2002; Prein and Gobiet, 2017; Rauthe et al., 2013).

At Rafina site, WRF simulated a rapid increase of 2 m air temperature and 10 m wind speed at 12Z on 23 July 2018 (Fig. 5) with a simultaneous decrease in relative humidity. In the model, the 2 m air temperature rose approximately 8 °C in twenty (20) minutes (from 11:45 UTC to 12:05 UTC, 23 July 2018), while according to the observational data a warming of 4 °C (6 °C) was recorded between 10:00 UTC and 10:30 UTC (11:30 UTC and 12:00 UTC). The maximum simulated (observed) air temperature at 2 m was 40.1 °C (39 °C) at 12:10 UTC (12:00 UTC). The observed maximum 10 min wind gust was 25.2 m s^{-1} against the modeled maximum wind speed of 17.5 m s^{-1}. However, the examination of the latter at time step intervals (wrfxtrm generated files) revealed values greater than 20 m s^{-1}.

In addition, the analysis on the simulated temperature field in the vertical showed that the aforementioned changes at Rafina site occurred close to the surface and up to ~800 m agl. The model results showed warming rates of 1 K min^{-1} (at ~800 m agl, 9th theta model level) to 4.3 K min^{-1} (at ~10 m agl, 1st theta model level), while the temperature begun to rise firstly aloft (11:35 UTC) and then at the lower levels (11:45 UTC). The wind speed followed the same temporal and vertical pattern but the onset of this increase took place earlier (11:30 UTC), almost 10 min prior to the temperature changes, implying vertical transport of energy and momentum from higher levels to the surface. Moreover, a decrease in wind speed magnitude was observed at all vertical levels close to the surface, prior to its intensification, which is related with the gradually change in wind speed direction. The maximum rate of the wind speed change was found equal to 10.7 m s^{-1}, at nearly 45 m agl.

The spatial analysis of the model results at the surface (Fig. 6a) reveals that at 09:00 UTC on 23/07, a pressure difference of ~3 hPa is established between northwest (higher pressures) and south east (lower pressures) of Gerania Mts (KINETA) and remains almost unchanged until the early evening hours. At the time of fire ignition at KINETA (~09:00 UTC), the simulated maximum wind speed is approximately 15 m s^{-1}, peaking its highest values (~18 m s^{-1}) at 12:45 UTC. Koletsis et al. (2009) noted also the existence of a pressure gradient during a downslope windstorm in Northwestern Greece, with maximum pressure difference of ~6 hPa. Moreover, at the greater area of MATI,
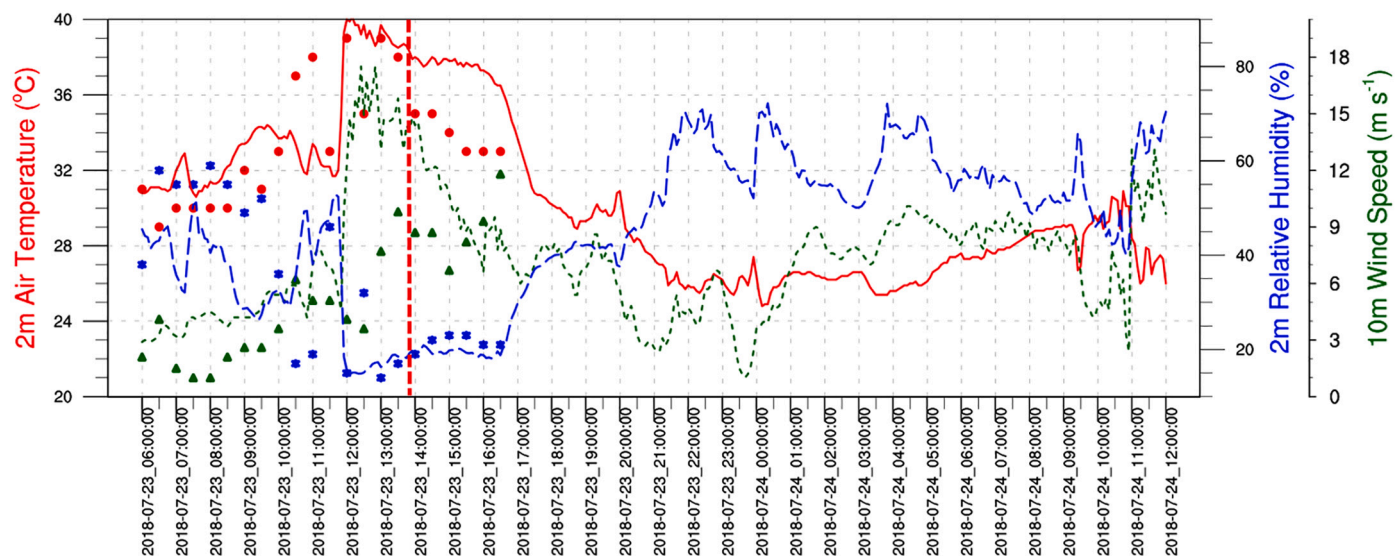
Table 2

The Mean Error (ME), Mean Absolute Error (MAE) and Root Mean Squared Error (RMSE) of the 2 m air temperature, 2 m relative humidity and 10 m wind speed at the locations of the 12 HNMS surface observations from 06Z 23/07/2018 to 12Z 24/07/2018 in CNTRL innermost (d03) domain. Also, the confidence intervals at the 95% significance level are shown.

	ME	MAE	RMSE
Tmp	1.4 ± 0.2	1.8 ± 0.1	2.2 ± 0.8
Rh	-3.7 ± 1.0	8.7 ± 0.7	11.6 ± 5.0
Wspd	1.9 ± 0.3	2.8 ± 0.2	3.6 ± 1.3

Fig. 5. Timeseries of 2 m air temperature (°C, red), 2 m relative humidity (%, blue) and 10 m wind speed (m s^{-1}, green) in WRF-d03 CNTRL simulation (solid, dashed lines) and HNMS observations (dots, asterisks, triangles) at Rafina (16793) site. The 10-min sustained observed wind speed is plotted. The WRF values were extracted by utilizing the IDW method. The vertical red dashed line indicates the time of fire ignition at MATI event. The time is in UTC.
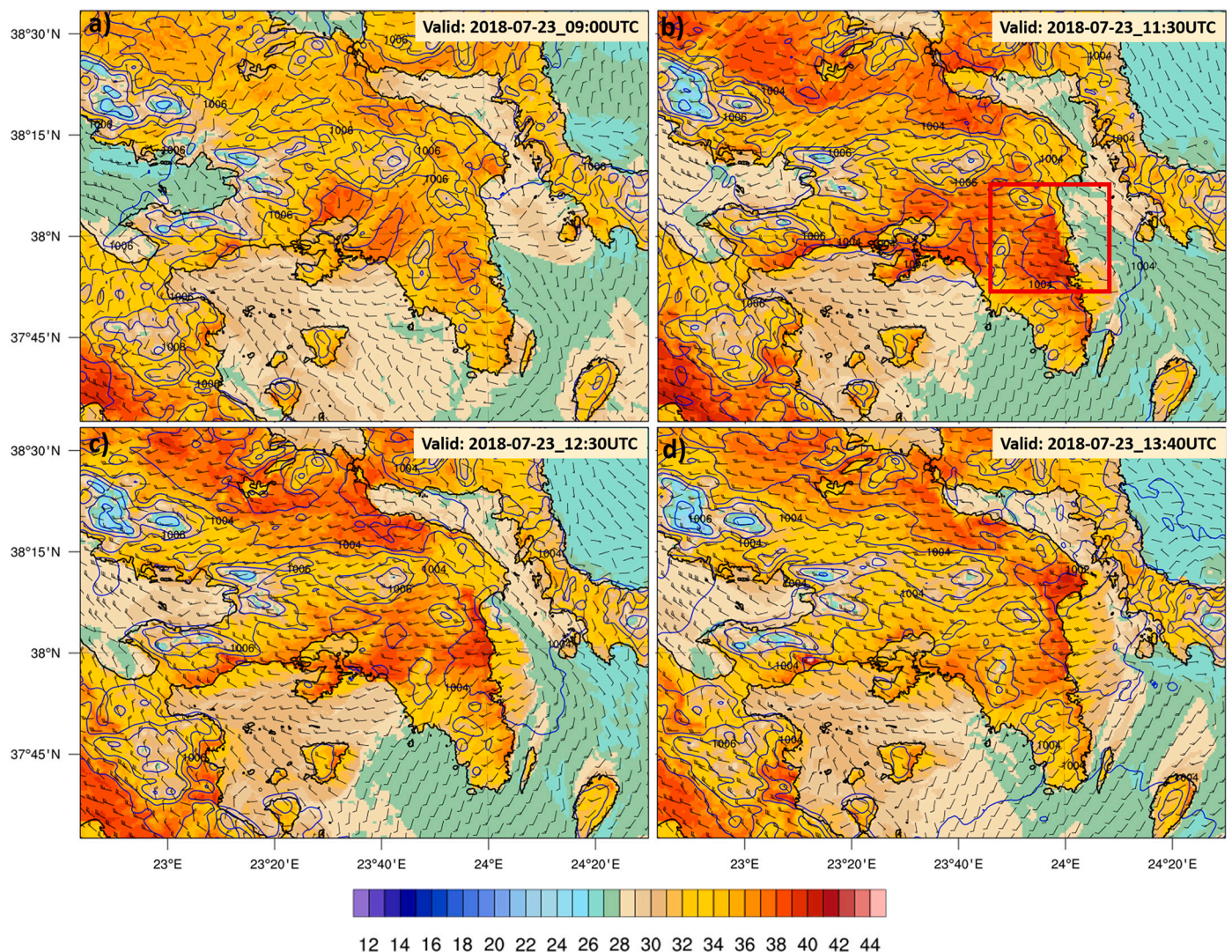

Fig. 6. Air temperature at 2 m (°C, shaded contours), mean sea-level pressure (hPa, blue contours) and 10 m wind speed (knots, windbarbs) at a) 09:00 UTC, b) 11:30 UTC, c) 12:30 UTC and d) 13:40 UTC on 23/07/2018, based on WRF-d03 values. Full windbarb = 10 knots, half windbarb = 5 knots.
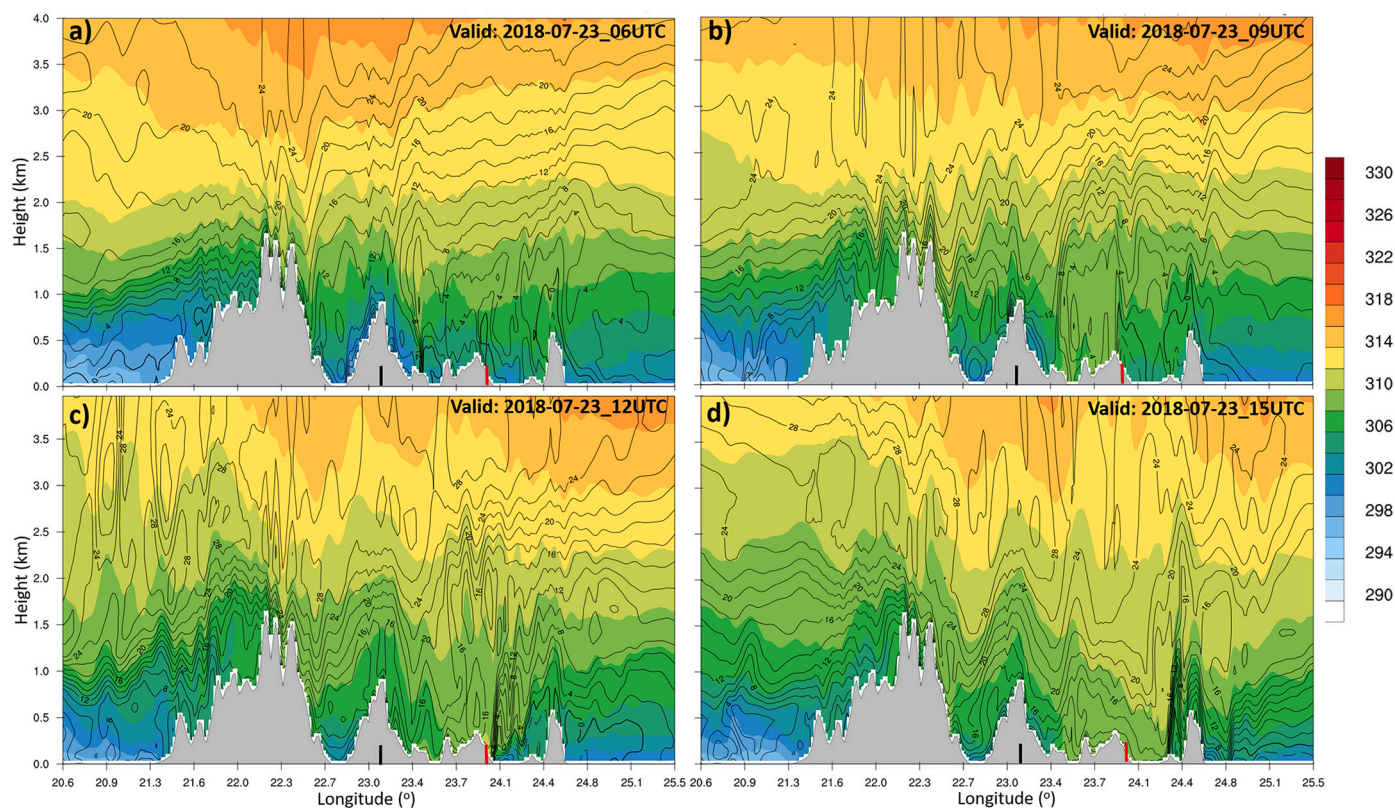
Fig. 7. Longitude - height sections of potential temperature (K, shaded contours) and u-component of wind speed (m s^{-1}, contours) at 38.035°N, on 23/07 at a) 06:00 UTC, b) 09:00 UTC, c) 12:00 UTC and d) 15:00 UTC, based on WRF-d02. See text for further details. Black and red line marks indicate the locations of Gerania Mts. and Penteli Mt., respectively.

the wind is blowing from east to east-southeast directions, with wind speed values below 5 m s^{-1} and without any significant pressure gradient. At 11:30 UTC (Fig. 6b), the prevailing weather conditions are characterized by strong westerly winds over the Attica region and high temperatures downwind of any orographic barrier. Worth of noting is the front-like feature of high temperatures at the vicinity of MATI, accompanied by high wind speeds with maxima of ~18 m s^{-1}, propagating eastwards towards the coast (red frame, Fig. 6b). Analysis of the simulated wind field at 10 m (not shown), revealed paths of strong localized and transient winds between Hymettus Mt. and Penteli Mt. Moreover, the aforementioned rapid increase of 2 m air temperature at Rafina site (Fig. 5) is clearly related with the passage of this feature. At the area of KINETA, the increase in temperature due to the wind field is also evident (Fig. 6a, b, c). The fire at Kallitehnoupolis (MATI event) (~13:49 UTC) ignited under strong westerlies (19 to 20 m s^{-1}), with relative humidity values less than 20% and ambient temperatures greater than 39 °C (Fig. 6d).

Fig. 7 displays the longitude – height section of potential temperature (K) and u-component of wind speed (m s^{-1}) from 06:00 UTC to 15:00 UTC at 3-hourly intervals, on 23/07. The aforementioned fields were extracted from the WRF-d02 intermediate nest (Fig. 2a) in order to highlight the effects of mountain chains, west of the Attica region, on the flow. In general, stable conditions are observed allowing for the development of mountain waves (Simpson et al., 2013b). The complex terrain at North Peloponnese (21.3°E to 22.7°E) seems to affect the atmospheric flow, gradually enhancing the vertical displacement of the air parcels (upwind phase tilt of the isotachs, Fig. 7a). As a result, orographic waves are formed leeward of the mountain range of North Peloponnese (Fig. 7b) in a layer between 1 and 3 km above the surface, while close to the ground the flow is characterized by locally induced variations (e.g. the easterly wind component at MATI location in Figs. 9b, c). At 12:00 UTC (Fig. Fig. 7c), the increase in zonal wind

speed is evident and strong downslope winds are dominating the lee-side of Gerania Mts (black short line), where the fire is active. Energy and momentum are propagating downwards into the lower troposphere, while a mid-level jet core lies from 3.5 to 5.5 km (not shown) and amplifying its strength from 13:00 UTC and onwards. Moreover, at the vicinity of MATI (red short line), a strong temperature and wind speed gradient is presented which coincides with the rapid increase of 2 m air temperature and 10 m wind speed as it was described earlier (Fig. 5, Fig. 6). During the fire event at MATI (Fig. 7d), the isotachs tilt in the vertical as they follow the descending part of the formed waves, resulting in strong katabatic winds and adiabatic heating of the lowest boundary layer in the region, as indicated by the isentropes.

The calculated omega (hPa hr^{-1}) values (Fig. 8) prior to the ignition times at both sites (09:00 UTC, KINETA; 13:40 UTC, MATI) declare strong downward motions (positive values) on the lee sides with a simultaneously decrease in water vapor mixing ratio, as drier air descents. This mechanism produces vertical mixing and thus the winds at lower levels inherit the characteristics of the wind field aloft, due to conservation of momentum (Sharples et al., 2012). At KINETA event, the model maintained these downward motions until the early night hours of 23/07, where the wind weakened significantly and turned into northerlies.

In addition, calculation of Richardson and Froude numbers (Fig. 9a, b) shows a transition from subcritical ($Fr < 1$) to supercritical ($Fr \geq 1$) flow on the lee slopes of Gerania Mts (KINETA) and Penteli Mt. (MATI) (Durran, 1990), while dynamically unstable and turbulent conditions ($Ri < 0.25$) are dominating at lower levels. At 09:00 UTC, 23/07/ 2018, the flow is subcritical ($Fr < 1$) over the area of interest (Attica region, 22.8°E – 24.1°E, Fig. 9a), with conversion of kinetic energy to potential energy (deceleration), as the air parcels ascent due to orography and vise-versa (acceleration) upon passing the crests. Upstream and aloft of Gerania Mts (Fig. 9c) static stability is positive, whereas
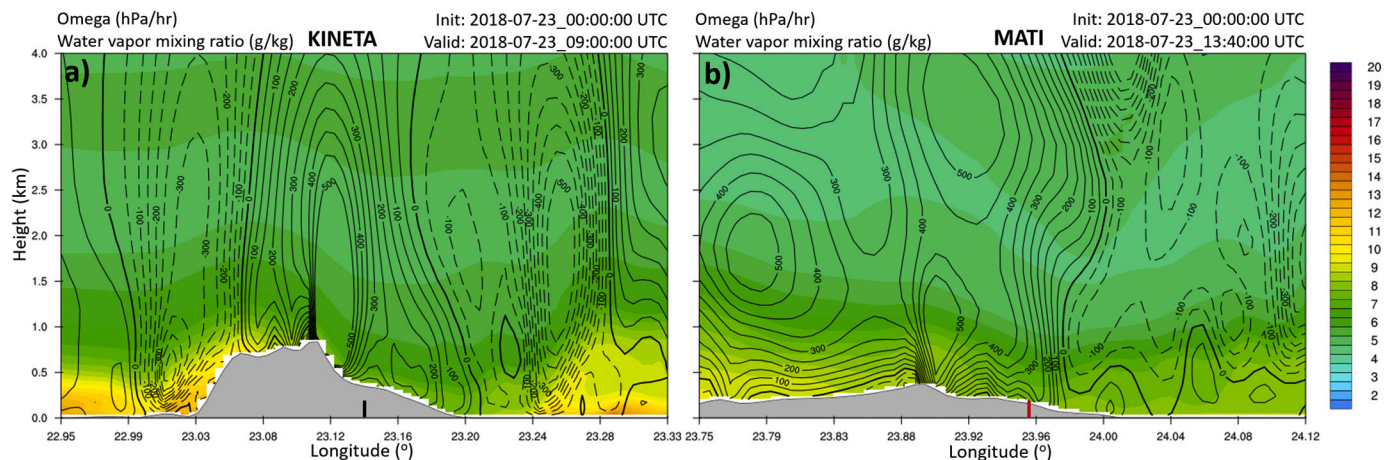
Fig. 8. a) Vertical cross-section through *E*-F dashed line (Fig. 2b) at 09:00 UTC, 23/07/2018 and b) G-H dashed line at 13:40 UTC, 23/07/2018 (Fig. 2b), of omega (hPa hr^{-1}, contours, positive values declare downward motions) and water vapor mixing ratio (g/kg, shaded contours) in WRF-d03. Black and red line marks indicate the locations of fire ignition at KINETA and MATI, respectively.

negative values (instability) are shown downwind. Moreover, the predicted wavelengths (contour lines, Fig. 9c, d) are close to the leeward slope widths (< 8 km) in the area, allowing for interaction between the mountain waves and the flow conditions downwind. At 12Z, the Froude number is approximately equal to unity over the crest of Gerania Mts and a supercritical regime eastwards is evident (23.1°E – 24.1°E, Fig. 9b), where the potential energy is converted into kinetic energy. This features is analogous to the hydraulic-like theory (Durran and Klemp, 1987; Smith, 1985), in which when the flow passes the top of the mountain, it accelerates further until the area referring as the hydraulic jump, where the flow turns back to the subcritical conditions

($Fr < 1$). In the case of 23rd of July 2018 at 12Z, this area is placed eastwards of Penteli Mt., as it can be shown in Fig. 9b.

It must be noted that, the hydraulic theory requires the determination of the top of the disturbed flow. According to Helmis et al. (2000) possible indicators can be the presence of a mean-state critical layer (Smith, 1985), a layer with decreased static stability with height or a temperature inversion (Durran, 1986; Klemp and Durran, 1987) or a wave-induced critical layer (wavebreaking, Klemp and Durran, 1987). Neither a mean-state critical level nor an inversion layer were not observed, which are important for the presence of vertical propagating mountain waves (Doyle and Jiang, 2006; Durran and Klemp, 1987;
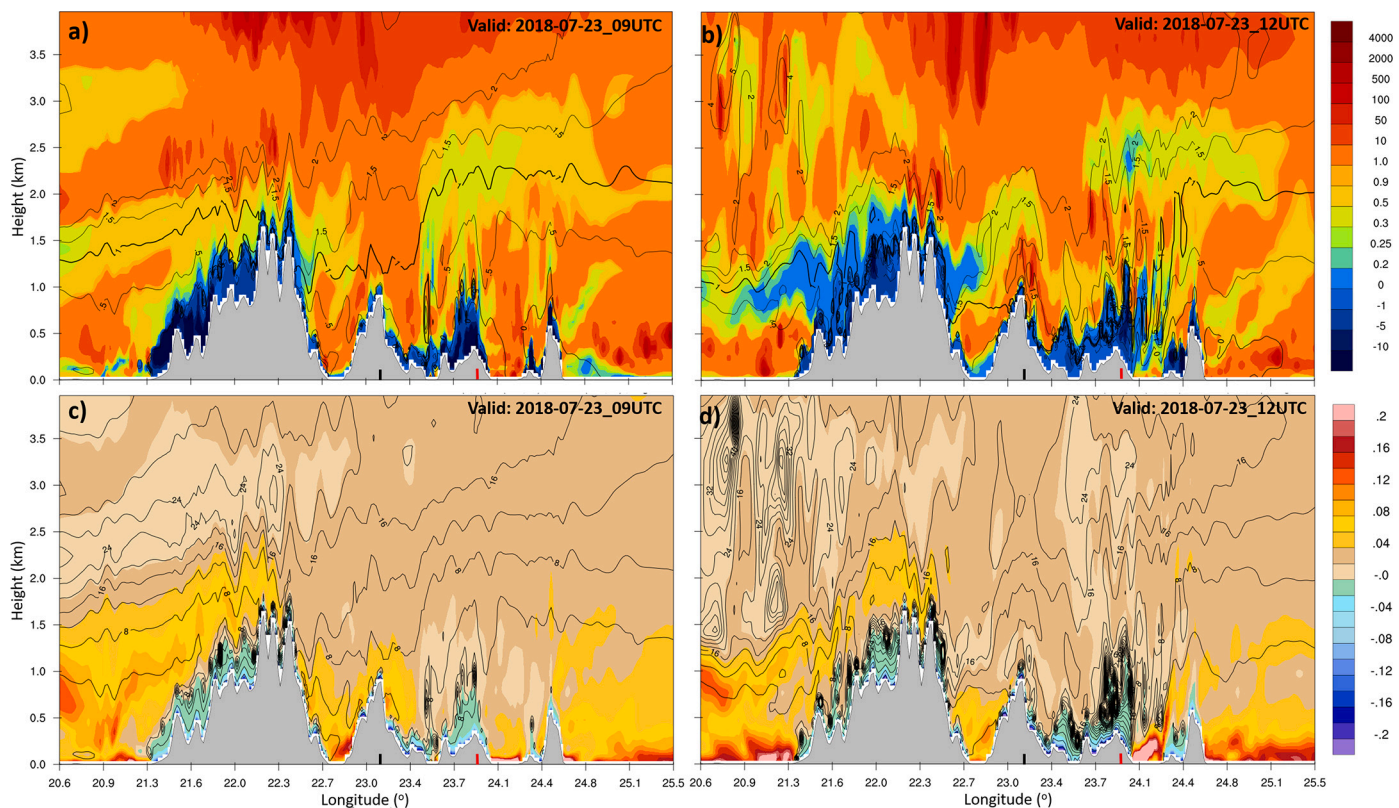

Fig. 9. Longitude - height sections of Richardson (shaded contours) and Froude (contours) numbers (top), static stability (K hPa^{-1}, shaded contours) and wavelengths (km, contours) (bottom) at 38.035°N, at a, c) 09:00 UTC and, b, d) 12:00 UTC, 23/07/2018, based on WRF-d02. Black and red line marks indicate the locations of Gerania Mts. and Penteli Mt., respectively.

Fudeyasu et al., 2008; Klemp and Lilly, 1975; Koletsis et al., 2009; Peltier and Clark, 1979). Although the current analysis reveal a vertical variation on the static stability with height over the area of interest (Fig. 9c, d), the flow dynamics involved are much more complicated and the hydraulic model can be utilized only in a qualitative manner (Durran, 1990; Helmis et al., 2000).

The resolved turbulent kinetic energy (TKE), averaged horizontally and vertically up to ~3600 m agl, from 23/07 at 06:00 UTC to 24/07 at 00:00 UTC over KINETA and MATI, was found equal to 0.31 and 0.37 m^2s^{-2}, respectively. The area under examination in both sites was defined downwind of Gerania Mts (28.7 km × 19.9 km, lon – lat) and Penteli Mt. (21.0 km × 20.5 km, lon – lat). The maximum averaged TKE at KINETA was 0.58 m^2s^{-2} (13:00 UTC) and 1.1 m^2s^{-2} at MATI (13:15 UTC), almost half an hour prior to the fire ignition at MATI event. The temporal examination of the averaged TKE at MATI revealed that values greater than 0.6 m^2s^{-2} encountered from 11:20 UTC to 15:35 UTC, implying that the fire ignited under turbulent conditions, which affected the fire spread. Also, the higher values of TKE at MATI are in line with the calculated Richardson number values (Fig. 9a, b), which were below the critical value of 0.25. Moreover, the maximum TKE in vertical at KINETA (MATI) was 14.67 (10.79) m^2s^{-2}.

4.2.2. Simulated fire behavior and evolution

The spatiotemporal evolution of the simulated fires at KINETA and MATI events was compared with fire data, derived from the 1-km spatial resolution MODIS Fire and Thermal Anomalies product (Giglio et al., 2003) and the corresponding Visible Infrared Imaging Radiometer Suite – VIIRS (Schroeder et al., 2014), at 375 m nominal resolution, while the simulated total burnt area in each event was compared with the Copernicus EMS-event EMSR300 data.

For KINETA, the total burnt area according to the WRF-SFIRE modelling system (from 23/07, 09:00 UTC until 24/07, 12:00 UTC) was 8336.82 ha (Table 3), approximately 48% greater than the observed one (5613.3 ha, Copernicus EMS-event EMSR300). It must be mentioned the different time period between the simulated and the observed fire event and the lack of temporal observation data regarding the actual burnt area. The mean rate of fire area growth was found equal to 0.04 ha/5 min, while the maximum accumulated heat fluxes from the fire were 245.3 MW m^{-2}, at 13:45 UTC. The rapid increase in the released heat fluxes since ignition, was simulated at approximately at 11:15 UTC and is associated with the ignition of an additional fuel type (NFFL fuel type 7, Southern rough) with high moisture of extinction values (~40%) and live foliage flammability (Anderson, 1982). In the case of the deadly fire at MATI, the fire model produced higher burnt area growth rates (average equal to 0.09 ha/5 min), representative of the actual fire propagation (Lekkas et al., 2018). The total modeled burnt area, at 00Z on 24/07, since ignition (23/07, ~13:49 UTC) was 1083.26 ha (Table 3), against 1275.9 ha, as recorded in the EMSR300 data (~ 84.9% of the observed burnt area). Also, two distinctive peaks in the heat fluxes from the fire at MATI (not shown) are presented, which slightly affected the burnt area growth rate. In both events, the fire area overpassed 10 ha almost two hours since ignition, due to the required time in order the model to develop a quasi-steady state fire. The latter is clearly shown in Fig. 10, where the temporal evolution of the simulated burnt area (solid lines), along with the observed hot spots from MODIS (green asterisks) and VIIRS (dots)

Table 3
Total burnt according to Copernicus EMS (event EMSR300) and WRF-SFIRE for KINETA and MATI fire events.

Wildland fire event	Total burnt area (ha)	
	EMSR300	WRF-SFIRE
KINETA	5613.3	8336.82
MATI	1275.9	1083.26

are depicted. At KINETA event (Fig. 10a), the simulated fire area (white solid line) is smaller than the area defined from the VIIRS thermal anomalies (white dots), at 11:40 UTC, on 23/07. The satellite data suggest that the fire front had reached the coastal area at that time, which cannot be confirmed at this point. However, it is possible that the VIIRS assigned as potential hot spots, locations along the smoke plume, with brightness temperatures greater than the applied thresholds in the VIIRS algorithm (Schroeder et al., 2014). As a result, the actual burnt area at that time might be much smaller, while worth of noting is that the WRF-SFIRE produced the VIIRS burnt area approximately two hours afterwards (red solid line), at 13:55 UTC. Some hours later, at 20:40 UTC, the predicted fire area (green solid line) is close to the MODIS product, where active fire fronts were observed along the western and eastern flanks. Similar fire behavior was observed during the Suomi-NPP satellite passage over the area, at ~00:05 UTC on 24/07, with the modeled burnt area (orange solid line) in good agreement with the active fire fronts (orange dots).

The fire ignition time at MATI along with the high propagation rates resulted to a limited number of satellite passes (only two), during this event. However, according to the MODIS Fire and Thermal Anomalies product (green asterisks, Fig. 10b), at 20:40 UTC, on 23/07, active fire fronts were spotted along the north and the southeast flanks, while the model produced an elongated fire area towards east (green solid line), which had arrived at the coastal area of Mati settlement. Despite the delay on the development of the fire momentum (dark blue solid line, Fig. 10b) and the late arrival time to the coast, the CNTRL simulation represented quite well the actual fire behavior, as the wind driven fire first reached to the sea and then started to spread laterally (orange dots and solid line, Fig. 10b). The WRF-SFIRE simulated the southward extent of the burnt area in very good agreement with the observations (orange vs blue solid line in Fig. 12b), but it did not manage to represent adequately the northward lateral propagation, due to the change in the modeled wind direction (westerlies to north-westerlies, not shown).

4.3. Sensitivity experiments

In this sub-section, the effect of topography on the local atmospheric conditions and thus on the fire behavior in both events is investigated. The weather and climate of the wider Attica region are dominated by its complex topographical features (Fig. 1), which influence the wind flow, altering its kinematic and dynamic characteristics.

In Fig. 11, vertical cross-sections of the 3-D wind speed (m s^{-1}, shaded contours) and potential temperature (K, contours) along the flow, in each site (columns; KINETA, left; MATI, right) and each experiment (rows; CNTRL, NTOPO, TOPOG and TOPOP) are shown. For the KINETA and MATI fire events, the cross-sections are along the E-F and G-H lines (Fig. 2b), respectively. According to the control simulation (CNTRL) and upon ignition time (23/07, 09Z) at KINETA (Fig. 11a), the flow at lower levels (which is from the left to the right of this section) decelerates upwind of Gerania Mts and accelerates on the lee of the mountain (values greater than 18 m s^{-1}), while a strong vertical wind shear is evident, with a local maximum greater than 36 m s^{-1} in the layer between 3.0 and 4.0 km. The isentropes rise and descent, following the terrain, where an unstable layer with near-adiabatic conditions (vertically tilted theta contours) close to the ground and upwind of the mountain is present but stable conditions are met downwind. The time evolution (not shown) revealed high wind peaks (greater than 16 m s^{-1}) and breaking offs (areas of low wind speed) downstream, until the late evening hours on 23rd of July 2018. By removing the topography in WRF-d03 (NTOPO), the isentropic lifting and descent weakens (Fig. 11c), the flow is more stratified in the lowest atmosphere, a very shallow layer with wind values between 14 m s^{-1} to 16 m s^{-1} lies above the ignition point, while the surface wind speed is less than 14 m s^{-1}. In addition, a region of strong static stability in the first 500 m above the surface is shown from 22.95°E to
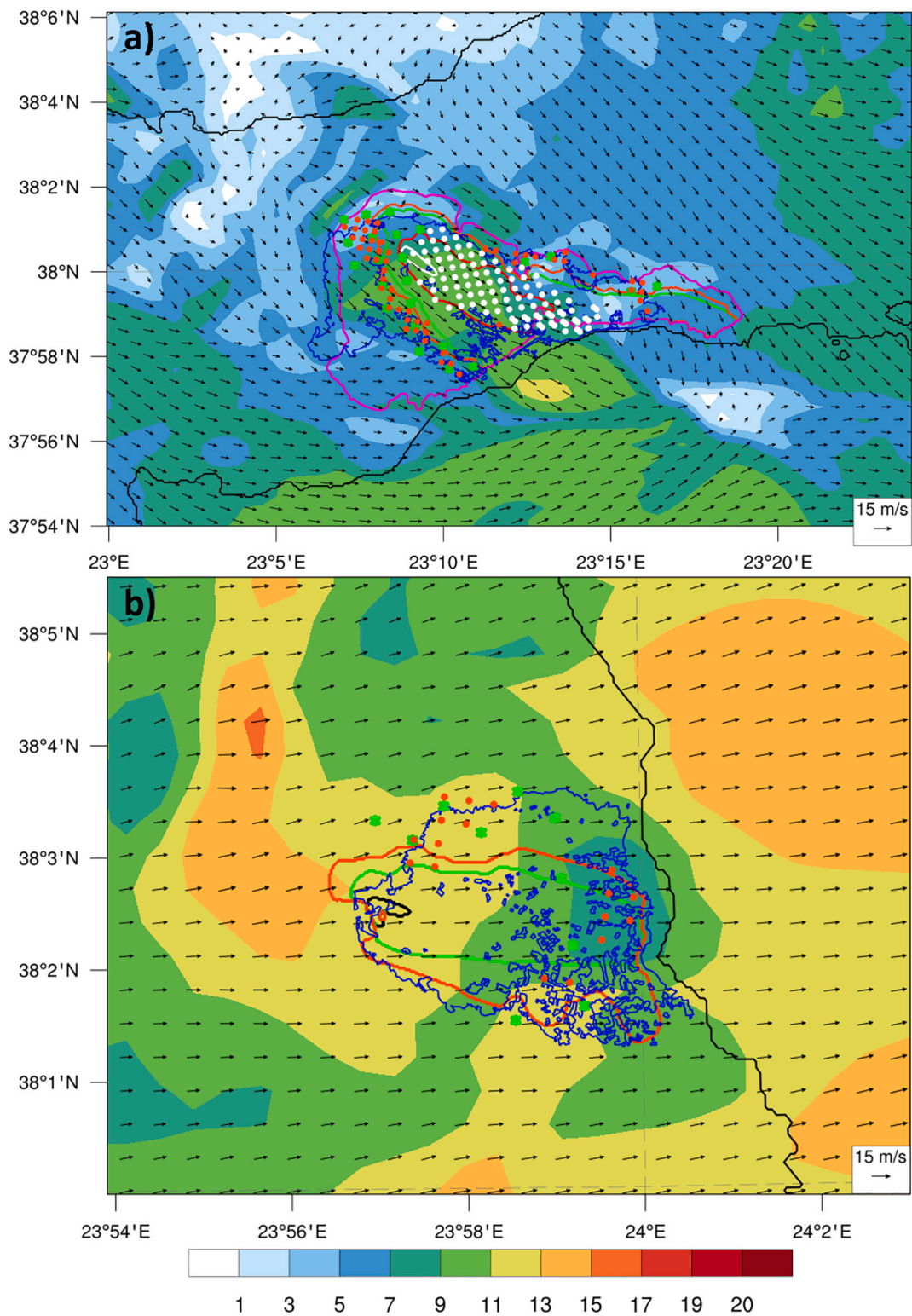
Fig. 10. Evolution of the simulated burnt area (solid lines) and the observed hot spots from MODIS (green asterisks) and VIIRS (dots), at a) KINETA and b) MATI fire events, in CNTRL experiment. Different dot, asterisk and line colors correspond to different times. At KINETA (a), white at 11:40 UTC, red at 13:55 UTC, green at 20:40 UTC, on 23/07 and orange at 00:05 UTC, magenta at 12:00 UTC, on 24/07. At MATI (b), dark blue at 16:30 UTC, green at 20:40 UTC, on 23/07 and orange at 00:00 UTC, on 24/07. The blue solid line illustrates the EMSR300 actual fire scar in both panels. The WRF-d03 simulated wind speed at fire wind height (6.096 m) (m s^{-1}, shaded contours) and direction (arrows), at a) 12:00 UTC 24/07 and b) 00:00 UTC 24/07 have been overplotted. A NCAR Command Language (NCL) thinning algorithm was applied in the number of arrows.

~23.08°E. In the TOPOG experiment (Fig. 11e), only the topography height of Gerania Mts was set equal to zero (KINETA black solid polygon line, Fig. 2b), in order to address the effects of the particular

barrier to the flow over the fire regime. By comparing the model results between NTOPO and TOPOG experiments, similarities arise, in both potential temperature and wind field, but a closer examination reveals

KINETA 2018-07-23_09:00 UTC   **MATI 2018-07-23_12:35 UTC**
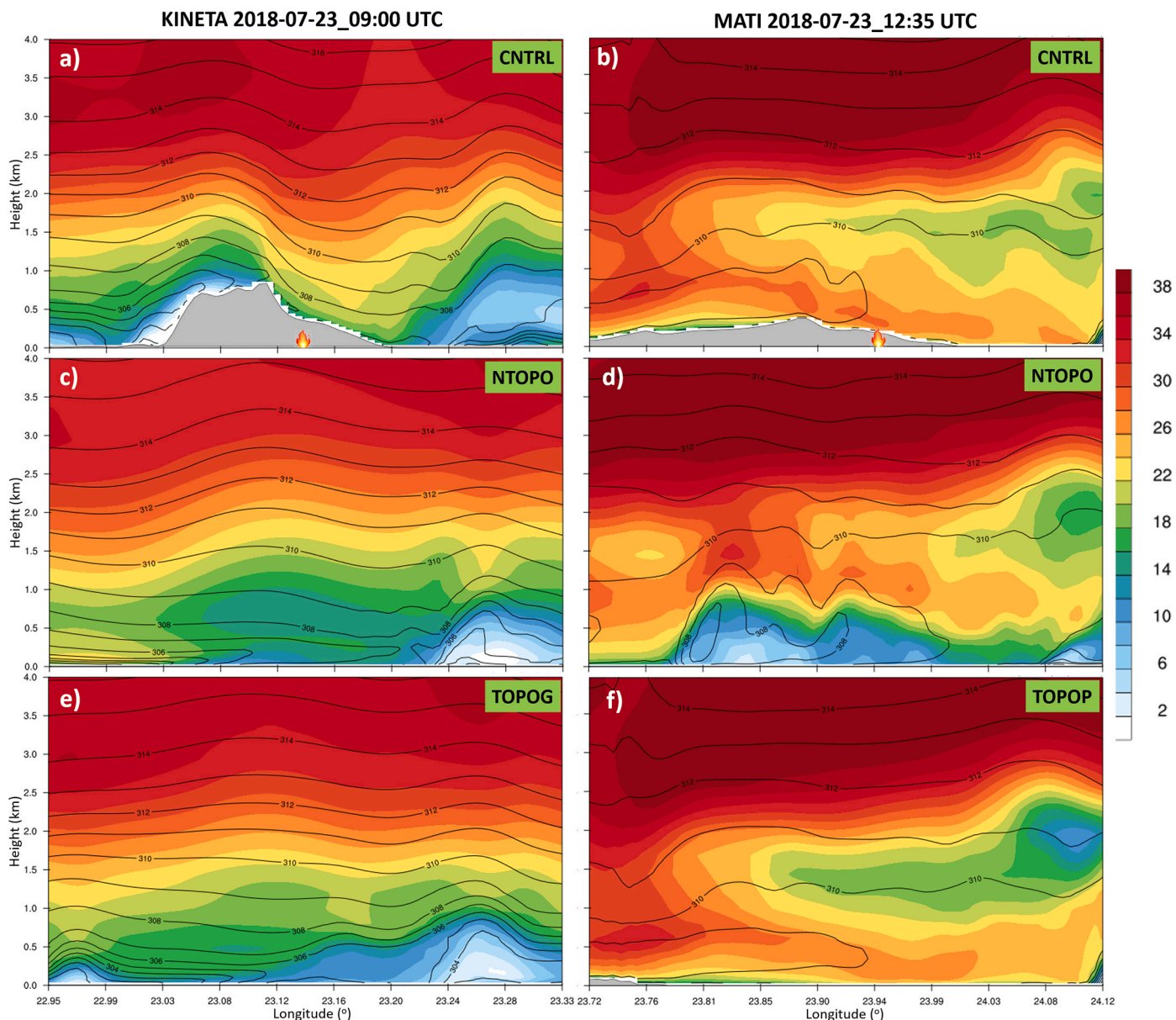

Fig. 11. Vertical cross-sections along E-F (left column, 09:00 UTC 23/07/2018) and G-H (right column, 13:45 UTC 23/07/2018) lines (Fig. 2b) of the 3-D wind magnitude (shaded contours) at 2 m s⁻¹ intervals and potential temperature (contours) at 1 K interval, at KINETA (left) and MATI (right) fire events, for control (CNTRL) simulation (a, b), NTOPO (c, d), TOPOG (e) and TOPOP (f) sensitivity experiments, based on WRF-d03. The fire symbols in (a) and (b) denote the location of fire ignition in each event.

that in TOPOG sensitivity run, colder air is advected over the fire area and more neutral conditions reside. The latter are attributed to the presence of the surrounding orographic barriers, which alter the flow over the fire region through canalization effects. Moreover, wind speed values below 12 m s⁻¹ are modeled and maintained throughout the 23rd of July 2018.

Approximately one hour before ignition time at MATI event, at 12:35 UTC (Fig. 11b), the flow in the control (CNTRL) simulation is neutrally stratified over the area of interest (23.94°E – 24.01°E), where two layers of high wind speeds are modeled. The upper layer lies above 2 km with jet core maxima over 38 m s⁻¹, while the lower layer is placed from the surface up to ~1 km, with local maximum above 32 m s⁻¹ (upstream of the ignition point). The flow is accelerated over the crest and downstream of Penteli Mt. (the cross-section is slightly to the south of the crest, G-F line in Fig. 2b), where peaks of high speeds are encountered resembling a hydraulic jump, albeit this feature was transient and presented only in the time window between 12Z to 13Z.

In this time slice, the highest modeled wind speeds at 10 m were also recorded at Rafina site (Fig. 5). In addition, the subsidence of the 310 K isentrope over the fire area (~1.5 km at 12:30 UTC and ~ 0.5 km at 14:05 UTC, not shown) along with the simultaneously wind speed increase at lower levels, indicates downward transport of momentum. In NTOPO experiment (Fig. 11d), the lack of any orography in the wider area of Attica resulted to increased stability followed by more neutral conditions at the time of the maximum wind speeds occurrence (~13:30 UTC to ~16:15 UTC). Although the two high wind speed regions are also resolved as in CNTRL, with nearly equal local maxima, the lower layer is located higher (1 km to 1.5 km agl), due to the presence of the warm front at ~23.81°E (Fig. 11d). In addition, the absence of topography in WRF-d03 increased the magnitude of the simulated low-level jet, located at around 0.5 km agl (not shown), with higher peak values (above 24 m s⁻¹, not shown) than in CNTRL (18–20 m s⁻¹, not shown). The modeled low-level jet appeared from ~17:00 UTC to ~19:00 UTC in both experiments. According to Fig. 11f,

Penteli Mt. (TOPOP) slightly modified the mean flow over the area of MATI. The TOPOP sensitivity experiment produced similar results with the CNTRL simulation, but on average introduced higher low-level jet speed values than in control run. Moreover, any resemblance of a hydraulic jump was not observed in TOPOP experiment.

The aforementioned results imply that Penteli Mt. might not have acted as the major contributor to the enhanced surface flow. Under strong background westerly flow, Hymettus Mt. could also produce intense downslope winds downwind of the mountain (Helmis et al., 2000), affecting the vicinity of the fire. A possible explanation would be that the interference of the produced waves, both from Hymettus and Penteli Mts, led to the local extrema in terms of the wind speed. If these assumptions were robust then the resolved wind speed maxima at NTOPO experiment would not be observed. On the contrary, the NTOPO simulation delivered wind speed values of the same magnitude as in the CNTRL. This suggests that, in general, the kinetic and dynamic characteristics of the mean flow over the Attica region were driven by the upper levels of the atmosphere, while the presence of the complex topography induced only spatiotemporal variations.

In order to evaluate how these topography induced variations affected the surface meteorological conditions in the vicinity of the MATI fire event, the 2 m air temperature, T2, (Fig. 12a), the 10 m wind speed, SPD, and direction, DIR, (Fig. 12b), in a WRF-d03 grid point with longitude-latitude values of 24.01633˚E, 38.00906ºN, from the control

(CNTRL) simulation, the NTOPO and TOPOP experiments, were extracted. The specific land point was selected as the closest to the sea grid point, in order to minimize the altitude effect on temperature between the three experiments. According to Fig. 12a, the temporal evolution (23/07_06Z to 24/07_00Z) of T2 in CNTRL and TOPOP was approximately the same. For the NTOPO simulation, the T2 presented higher values at morning hours (06:00 UTC to 08:30 UTC, i.e. 09:00 to 11:30 local time), due to the prevailing westerlies (Fig. 12b, orange diamonds) which were advecting warm air from the inland, while the rapid rise in temperature (dashed orange line, Fig. 12a) resulted almost one hour prior to the corresponding one in the control (CNTRL) simulation. The latter shows that topography did not contribute to the mechanism behind this increase, rather it delayed its occurrence. From 06:00 UTC to ~11:30 UTC, on 23 July 2018, the NTOPO wind speed (dashed orange line, Fig. 12b) was higher than in CNTRL and TOPOP (expect at some instances where the change in wind direction occurred), but lower in the time window between 11:50 UTC to 14:05 UTC, in which the CNTRL and TOPOP SPD maxima were presented. Moreover, the lack of Penteli Mt. (red dotted line, Fig. 12b) allowed the south-easterlies to maintain their strength until ~11:45 UTC, as they were penetrating towards the inland.

Fig. 13 presents the predicted fire perimeter as obtained from the control simulation (black solid line), the NTOPO (orange solid line), the TOPOG and TOPOP (red solid line) experiments, along with the
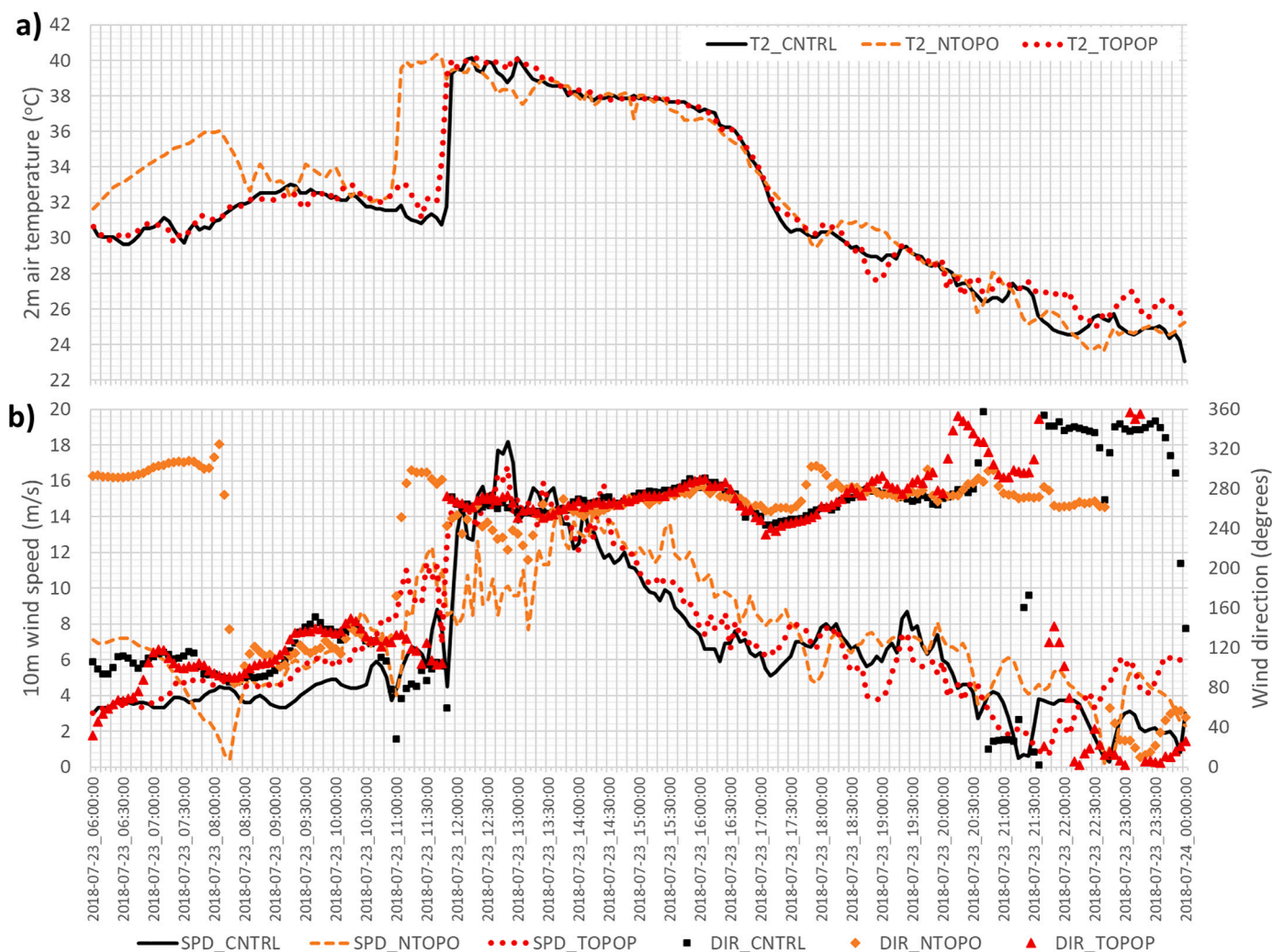

Fig. 12. Timeseries of a) air temperature at 2 m (°C), b) wind speed (SPD; m s^{-1}) and direction (DIR; degrees) at 10 m, at the WRF-d03 grid point with longitude-latitude values of 24.01633˚E, 38.00906ºN (in the area of MATI's fire event), from CNTRL (black solid lines, black squares), NTOPO (orange dashed lines, orange diamonds) and TOPOP (red dotted lines, red triangles) experiments. The time is in UTC.
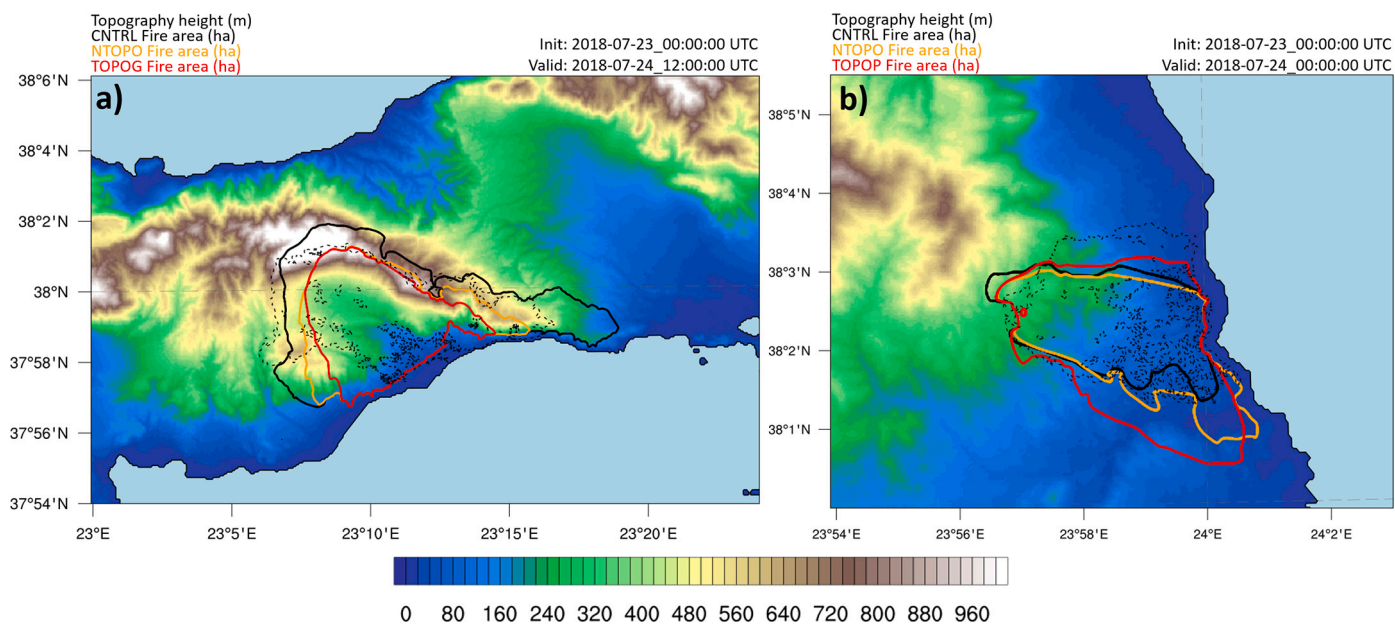
Fig. 13. Topography height (m; shaded contours), EMSR300 fire perimeter (black dashed line) and predicted burnt area in control (black solid line), NTOPO (orange solid line), TOPOG and TOPOP (red solid line) experiments for the a) KINETA (12:00 UTC, 24/07/2018) and b) MATI (00:00 UTC, 24/07/2018) fire events, respectively.

observed EMSR300 burnt area (black dashed line) and the SRTM topography height (m; v3; 30 m × 30 m; shaded contours), for a) KINETA (12Z, 24/07) and b) MATI fire events (00Z, 24/07). The previously presented analysis, in terms of vertical cross sections of potential temperature and 3-dimensional wind speed over the areas of interest, 2 m air temperature and 10 m wind grid point values, is reflected to the predicted fire area at KINETA (Fig. 13a), in both sensitivity experiments (NTOPO, TOPOG). Gerania Mts contributed positively to warmer and drier surface conditions, enhanced the flow downstream, while the barrier produced and transported turbulence over the vicinity of the fire. As a result, the largest predicted fire area was presented in the CNTRL simulation (8336.82 ha). The lack of any topographical feature in the region of the innermost domain (NTOPO) led to smaller fire area (5265.29 ha) than in the control simulation, which justifies the aforementioned. Moreover, the removal of only the Gerania Mts. (TOPOG) resulted in the smallest burnt area (4327.94 ha) in total, which is about half of the predicted fire perimeter in the CNTRL experiment. The larger fire area in NTOPO compared to TOPOG sensitivity run is attributed to a) warmer and drier conditions overall in NTOPO and b) to the difference in wind direction (NTOPO, north-northwest; TOPOG northwest) during the morning hours of 24th of July 2018 and until the end of the simulation (12Z, 24/07). The latter allowed faster lateral fire spread on the southwest flank (orange line, Fig. 13a) against the TOPOG run. In addition, the NTOPO northeast flank experienced faster spread rates since ignition, due to the west-northwest wind direction, whereas in the TOPOG experiment the wind blew mostly from northwest directions (not shown).

On the contrary, the topography at MATI event negatively affected the extent of the burnt area, where the absence of either the orograph of the region covered by WRF-d03 (NTOPO) or only Penteli Mt. (TOPOP) led to larger burnt areas against the CNTL run (Fig. 13b). In each experiment, the fire propagation was driven by the mean flow, which was affected by the morphological characteristics of the surroundings. In CNTRL simulation, the fire initially spread towards east (approximately until 19Z on 23/07), while it developed an eastward-northeastward (eastward-southeastward) direction in NTOPO (TOPOP). At 20Z, on 23/07, the CNTRL fire perimeter matched with the NTOPO burnt area (not shown), due to the presence of a northwesterly flow descending from Penteli Mt. (in CNTRL), but overall, the higher NTOPO wind speed

values since ignition, emanating from the lack of topography, contributed to faster burning rates (2.0 ha/5 min against 1.8 ha/5 min, temporal mean from 13:50 to 23:55 UTC, 23/07). At the same time, in TOPOP experiment, a convergence region (with local maximum of ~15 s^{-1}) over the fire area (not shown) led to an escalating fire behavior (2.8 ha/5 min, temporal mean from 13:50 to 23:55 UTC, 23/07), albeit it moved southwards and dissipated in the following hours. As a result, the TOPOP burnt area presented an extended south flank (red line, Fig. 13b) at 00Z, on 24th of July 2018 in contrast to the CNTRL fire area.

5. Summary and conclusions

This study presented the prevailing synoptic and surface weather conditions on 23rd of July 2018, in which two devastating fires ignited at Attica region, with 102 fatalities during the deadly fire at MATI event. It also examined the role of topography on the modification of the mean flow and its impact on the fire behavior in each event, through a number of high-resolution numerical experiments.

At MATI event, the extreme windy conditions in conjunction with the morphological features of the area (wildland-urban interface) resulted in aggressive spread rates and fire behavior, burning 1275.9 ha in total, until the early hours on 24th of July 2018. According to HNMS weather station data at Rafina site, which was destroyed by the fire, on 23/07 the maximum recorded temperature was 39 °C, the sustained wind speed reached 11.8 m s^{-1}, with maximum gustiness of 25.2 m s^{-1}. The fire at Gerania Mts. (KINETA) was maintained until the late hours on 25th of July 2018, where the fire area was 5613.3 ha, as obtained from the Copernicus EMS – Mapping platform.

The online coupled WRF-SFIRE modelling system was utilized in order to simulate these two extreme fire events, analyze the prevailing synoptic and local atmospheric conditions and examine the impact of complex terrain to the mean flow and fire behavior. The model was validated in terms of temperature, relative humidity and wind speed against the available HNMS surface observations and found to be consistent with the literature.

The unavailability of radiosonde data and surface observations from a denser weather station network set some limitations to the analysis of the meteorological conditions that affected the fire propagation.

Although the model errors align with the bibliography for the wider area of Mediterranean region, they can be attributed to several factors. Karacostas et al. (2018) showed that the upper-air synoptic circulation type plays an important role in the performance of the WRF model. In addition, initialization errors due to the low density of surface and upper-air observations in the wider area, deficiencies in the representation of the physical mechanisms and in morphological features (e.g. topography, land uses) are some possible reasons contributing to the above discrepancies. In addition, the meteorological numerical experiments were performed at high horizontal resolution (WRF-d03: dx = dy = 0.555 km), where predictability decreases as one approaches the threshold resolution of an explicit simulation of boundary layer processes deterministically (Mukherjee et al., 2016).

The examination of the physical processes that produced such windy conditions on the leeward slopes of Gerania Mts. and Penteli Mt., on 23rd of July 2018, did not reveal any distinctive mechanism involved. However, the lower atmosphere was subjected to vertical oscillations, where the complex terrain modified the mean airflow by inducing orographic waves, with wavelengths below 2 km. The presence of vertically propagating mountain waves requires specific criteria to be met. The control simulation (sub-section 4.2) did not resolve, either a mean-state critical level (reversed flow or mean flow equal to zero) or an inversion layer, albeit a vertical variation on the static stability with height was observed. The altered airflow showed also a transient resemblance of a hydraulic jump downstream of Penteli Mt. (MATI), while on the lee-slopes of Gerania Mts. (KINETA) a strong vertical wind shear was evident. Moreover, the numerical simulations presented a sinking on the isotachs over the Attica region, where the highest wind speeds were simulated. Although this feature needs further investigation, it is associated with downward transport of energy and momentum, as the subtropical jet passed over Central Greece. As a result, the question whether the hydraulic or vertically propagating wave theory applies in this case can be answered only in a qualitatively manner.

The effect of topography to fire behavior found to be different in the two cases. The isolated Gerania Mts. (KINETA event) influenced the lee-slope surface winds in a more linear way, where the presence of the particular barrier clearly enhanced the katabatic flow, which led to warmer and drier conditions at surface and thus affected the predicted total burnt area. On the other hand, Penteli Mt. (MATI event) contributed to the modification of the flow in the vicinity of the fire non-linearly, due to the surrounding complex terrain. The analysis indicated possible interferences on the flow by Hymettus Mt. or other barriers upstream (e.g. Parnitha Mt.), which either amplified or diminished the surface winds in the sensitivity experiment (TOPOP).

The coupled model was able to reproduce the total burnt area in each event in a satisfactory way, taking advantage of the wind-driven propagation, where the fire behavior is mainly controlled by the mean flow (Morvan, 2011). In both fire events, the modeled fire required a "spin-up" time in order to develop a quasi-steady state, therefore discrepancies occurred in the temporal evolution of the predicted fire mostly at MATI event, as the fire module failed to represent the aggressive fire propagation. Given that the highest surface winds were simulated during this "spin-up" period, the mismatch in fire spread rates is reasonable. Although, the same "delay" was also presented in the fire at Gerania Mts.(KINETA), it had a smaller impact on its temporal evolution as the sustained windy conditions affected the propagation rates longer due to its earlier ignition time.

The 1 to 20 ratio between atmospheric and fire mesh, led to a horizontal discretization of approximately 30 m × 30 m for the fire model, which is close to the available topographical SRTM data. Despite the very fine resolution, certain physical processes regarding the atmosphere-fire interactions were not resolved, such as the observed (Sentinel 2A) lateral fire spread at KINETA event (not shown), revealing potential limitations due to relative coarse resolution for these processes.

Another factor that adds limitations and inherits errors to the predicted fire is that the fire model (SFIRE) represents fire propagation only as surface fire (Mandel et al., 2011). In fact, the deadly fire at East Attica region (MATI event) was characterized as canopy fire, at least upon arrival at the wildland-urban interface of Neos Voutzas, Rafina, Mati and Kokkino Limaki settlements, which contributed to extreme spread rates and fire spotting (Egorova et al., 2019; Fernandez-Pello, 2017). In addition, the empirical fire spread formula (Rothermel, 1972) have not been validated at high wind speeds (Coen et al., 2018), while there is a hardcoded upper limit (6 m s^{-1}) in the predicted rate of spread (ROS) inside the fire module.

It is evident that the representation of the fuel conditions greatly affected the modeled fire behavior, where additional sensitivity experiments revealed the need for the applied fuel model reclassification in the area of MATI event. Recently, two studies (Giannaros et al., 2019; Lagouvardos et al., 2019) investigated the performance of WRF-SFIRE modelling system in the case of MATI event. As they were closely related to each other, both studies utilized a fuel representation dataset, based on Scott and Burgan (2005) fuel models and additional custom fuels, albeit that dataset was constructed on relatively coarse resolution (100 m × 100 m).

Moreover, the conversion and resampling of the relatively coarse resolution CORINE land use data (100 m × 100 m) into NFFL fuel models (30 m × 30 m) introduced errors, as the actual sub-grid variability in the fuel composition was not reflected inside the model, while the fuel moisture was tuned through the activation of the embedded fuel moisture model (Mandel et al., 2014), with no further adjustment. Even though the aforementioned conversion was based on literature, it stresses out the need for a common strategy regarding the mapping and representation of fuels at national level. Finally, the fire model did not account for fire-fighting operations, which play an important role in the shape of the final burnt area, albeit in the case of the MATI fire event, the response time was very limited.

Declaration of Competing Interest

The authors declare that they have no known competing financial interests or personal relationships that could have appeared to influence the work reported in this paper.

cover data (https://land.copernicus.eu/pan-european/corine-land-cover, last accessed 28/06/2020). Moreover, we acknowledge the products of NASA, especially the Fire Thermal Anomalies dataset (https://modis.gsfc.nasa.gov/data/dataprod/mod14.php, last accessed 28/06/2020) and the Shuttle Radar Topography Mission dataset (https://www2.jpl.nasa.gov/srtm/, last accessed 28/06/2020). Finally, we acknowledge the Earth Science Data and Information System (ESDIS) Project (https://earthdata.nasa.gov/esdis, last accessed 28/06/2020) and the Visible Infrared Imaging Radiometer Suite (VIIRS). For analysis and visualization purposes, the NCAR Command Language (NCL; v.6.6.2) and Microsoft Office were utilized. The resampling of land use data to fuel models was performed in Quantum GIS (v.2.18.16). Finally, we would like to thank the two anonymous reviewers for their constructive review.

Appendix A. Supplementary data

Supplementary data to this article can be found online at https://doi.org/10.1016/j.atmosres.2020.105253.

References

Ahmad, F., Goparaju, L., 2019c. Forest Fire Trend and Influence of Climate Variability in India: A Geospatial Analysis at National and Local Scale. Ekol. Bratislava 38, 49–68. https://doi.org/10.2478/eko-2019-0005.

Ahmad, F., Goparaju, L., Qayum, A., 2018. Himalayan forest fire characterization in relation to topography, socio-economy and meteorology parameters in Arunachal Pradesh, India. Spat. Inf. Res. 26, 305–315. https://doi.org/10.1007/s41324-018-0175-1.

Ahmad, F., Uddin, M.M., Goparaju, L., 2019a. Fire risk assessment along the climate, vegetation type variability over the part of Asian region: a geospatial approach. Model. Earth Syst. Environ. 5, 41–57. https://doi.org/10.1007/s40808-018-0517-y.

Ahmad, F., Uddin, M.M., Goparaju, L., 2019b. Evaluation of long term forest fires in India with respect to state administrative boundary, forest category of LULC and future climate change scenario: A Geospatial Perspective. For. Res. Pap. 79, 335–343. https://doi.org/10.2478/frp-2018-0034.

Amraoui, M., Liberato, M.L.R., Calado, T.J., DaCamara, C.C., Coelho, L.P., Trigo, R.M., Gouveia, C.M., 2013. Fire activity over Mediterranean Europe based on information from Meteosat-8. For. Ecol. Manag. 294, 62–75. https://doi.org/10.1016/J.FORECO.2012.08.032.

Amraoui, M., Pereira, M.G., DaCamara, C.C., Calado, T.J., 2015. Atmospheric conditions associated with extreme fire activity in the Western Mediterranean region. Sci. Total Environ. 524–525, 32–39. https://doi.org/10.1016/j.scitotenv.2015.04.032.

Anderson, H.E., 1970. Forest fuel ignitibility. Fire Technol. 6, 312–319. https://doi.org/10.1007/BF02588932.

Anderson, H.E., 1982. Aids to determining fuel models for estimating fire behavior. Bark Beetles, Fuels, Fire Bibliogr. 1–22 (citeulike-article-id:12114185).

Barry, R.G., 1992. Mountain Weather and Climate, 2nd ed. Routledge, New York.

Baughman, R.G., Albini, F.A., 1980. Estimating midflame windspeeds. In: Sixth Conference on Fire and Forest Meteorology. Seatle. WA, pp. 88–92.

Benali, A., Ervilha, A.R., Sá, A.C.L., Fernandes, P.M., Pinto, R.M.S., Trigo, R.M., Pereira, J.M.C., 2016. Deciphering the impact of uncertainty on the accuracy of large wildfire spread simulations. Sci. Total Environ. 569–570, 73–85. https://doi.org/10.1016/j.scitotenv.2016.06.112.

Bluestein, H.B., 1992. Synoptic-Dynamic Meteorology in Midlatitudes: Principles of Kinematics and Dynamics. Oxford University Press, New York.

Brown, J.K., 1970. Ratios of Surface Area to Volume for Common Fine Fuels. For. Sci. 16, 101–105. https://doi.org/10.1093/FORESTSCIENCE/16.1.101.

Butler, B.W., Bartlette, R.A., Bradshaw, L.S., Cohen, J.D., Andrews, P.L., Putnam, T., Mangan, R.J., 1998. Fire behavior associated with the 1994 South Canyon fire on Storm King Mountain, Colorado. Ogden, UT. https://doi.org/10.2737/RMRS-RP-9.

Chen, F., Dudhia, J., 2002. Coupling an advanced land surface–hydrology model with the Penn State–NCAR MM5 modeling system. Part II: preliminary model validation. Mon. Weather Rev. 129, 587–604. https://doi.org/10.1175/1520-0493(2001)129<0587:caalsh>2.0.co;2.

Clark, T.L., Peltier, W.R., 1984. Critical Level Reflection and the Resonant Growth of Nonlinear Mountain Waves. J. Atmos. Sci. 41, 3122–3134. https://doi.org/10.1175/1520-0469(1984)041<3122:CLRATR>2.0.CO;2.

Coen, J., Schroeder, W., Quayle, B., Coen, J.L., Schroeder, W., Quayle, B., 2018. The Generation and Forecast of Extreme Winds during the Origin and Progression of the 2017 Tubbs Fire. Atmosphere (Basel) 9, 462. https://doi.org/10.3390/atmos9120462.

Dimitrakopoulos, A.P., Panov, P.I., 2001. Pyric properties of some dominant Mediterranean vegetation species. Int. J. Wildl. Fire 10, 23. https://doi.org/10.1071/WF01003.

Dobrinkova, N., Jordanov, G., Mandel, J., 2011. WRF-Fire Applied in Bulgaria, in: Lecture Notes in Computer Science (Including Subseries Lecture Notes in Artificial Intelligence and Lecture Notes in Bioinformatics). https://doi.org/10.1007/978-3-642-18466-6_15.

Doyle, J.D., Durran, D.R., 2004. THE MAP ROOM: Recent Developments in the Theory of Atmospheric Rotors. Bull. Am. Meteorol. Soc. 85, 337–342. https://doi.org/10.1175/BAMS-85-3-337.

Doyle, J.D., Jiang, Q., 2006. Observations and numerical simulations of mountain waves in the presence of directional wind shear. Q. J. R. Meteorol. Soc. 132, 1877–1905. https://doi.org/10.1256/qj.05.140.

Duguy, B., Alloza, J.A., Röder, A., Vallejo, R., Pastor, F., 2007. Modelling the effects of landscape fuel treatments on fire growth and behaviour in a Mediterranean landscape (eastern Spain). Int. J. Wildl. Fire 16, 619. https://doi.org/10.1071/WF06101.

Durran, D.R., 1986. Another look at Downslope Windstorms. Part I: the Development of Analogs to Supercritical Flow in an Infinitely deep, Continuously Stratified Fluid. J. Atmos. Sci. 43, 2527–2543. https://doi.org/10.1175/1520-0469(1986)043<2527:ALADWP>2.0.CO;2.

Durran, D.R., 1990. Mountain Waves and Downslope Winds, in: Atmospheric Processes over Complex Terrain. American Meteorological Society, Boston, MA, pp. 59–81. https://doi.org/10.1007/978-1-935704-25-6_4.

Durran, D.R., Klemp, J.B., 1987. Another look at Downslope Winds. Part II: Nonlinear Amplification beneath Wave-Overturning Layers. J. Atmos. Sci. 44, 3402–3412. https://doi.org/10.1175/1520-0469(1987)044<3402:ALADWP>2.0.CO;2.

Egorova, V.N., Trucchia, A., Pagnini, G., 2019. Fire-spotting generated fires. Part I: The role of atmospheric stability. Appl. Math. Model. https://doi.org/10.1016/J.APM.2019.02.010.

Farguell, À., Cortés, A., Margalef, T., Miro, J.R., Mercader, J., 2017. Data resolution effects on a coupled data driven system for forest fire propagation prediction. Procedia Comput. Sci. 108, 1562–1571.

Farr, T.G., Rosen, P.A., Caro, E., Crippen, R., Duren, R., Hensley, S., Kobrick, M., Paller, M., Rodriguez, E., Roth, L., Seal, D., Shaffer, S., Shimada, J., Umland, J., Werner, M., Oskin, M., Burbank, D., Alsdorf, D., 2007. The Shuttle Radar Topography Mission. Rev. Geophys. 45, RG2004. https://doi.org/10.1029/2005RG000183.

Fernandez-Pello, A.C., 2017. Wildland fire spot ignition by sparks and firebrands. Fire Saf. J. 91, 2–10. https://doi.org/10.1016/J.FIRESAF.2017.04.040.

Fosberg, M.A., 1983. Weather in Wildland Fire Management: The Fire Weather Index. Conference on Sierra Nevada Meteorology Lake Tahoe, CA, USA.

Founda, D., Giannakopoulos, C., 2009. The exceptionally hot summer of 2007 in Athens, Greece — A typical summer in the future climate? Glob. Planet. Change 67, 227–236. https://doi.org/10.1016/j.gloplacha.2009.03.013.

Fudeyasu, H., Kuwagata, T., Ohashi, Y., Suzuki, S., Kiyohara, Y., Hozumi, Y., 2008. Numerical Study of the Local Downslope Wind "Hirodo-Kaze" in Japan. Mon. Weather Rev. 136, 27–40. https://doi.org/10.1175/2007MWR2049.1.

Giannaros, T.M., Kotroni, V., Lagouvardos, K., 2019. IRIS – Rapid response fire spread forecasting system: Development, calibration and evaluation. Agric. For. Meteorol. 279, 107745. https://doi.org/10.1016/J.AGRFORMET.2019.107745.

Giglio, L., Descloitres, J., Justice, C.O., Kaufman, Y.J., 2003. An Enhanced Contextual Fire Detection Algorithm for MODIS. Remote Sens. Environ. 87, 273–282. https://doi.org/10.1016/S0034-4257(03)00184-6.

Haines, D.A., Lyon, L.J., 1990. Horizontal roll vortices in complex terrain. Fire Manag. notes U.S. Dep. Agric. For. Serv.

Haylock, M.R., Hofstra, N., Klein Tank, A.M.G., Klok, E.J., Jones, P.D., New, M., 2008. A European daily high-resolution gridded data set of surface temperature and precipitation for 1950–2006. J. Geophys. Res. 113, D20119. https://doi.org/10.1029/2008JD010201.

Helmis, C.G., Flocas, H.A., Kalogiros, J.A., Asimakopoulos, D.N., 2000. Strong downslope winds and application of hydraulic-like theory. J. Geophys. Res. Atmos. 105, 18039–18051. https://doi.org/10.1029/2000JD900246.

Iacono, M.J., Delamere, J.S., Mlawer, E.J., Shephard, M.W., Clough, S.A., Collins, W.D., 2008. Radiative forcing by long-lived greenhouse gases: Calculations with the AER radiative transfer models. J. Geophys. Res. 113, D13103. https://doi.org/10.1029/2008JD009944.

Isaaks, E.H., Srivastava, R.M., 1989. An Introduction to Applied Geostatistics.

Janjić, Z.I., 1994. The Step-Mountain Eta Coordinate Model: Further Developments of the Convection, Viscous Sublayer, and Turbulence Closure Schemes. Mon. Weather Rev. 122, 927–945. https://doi.org/10.1175/1520-0493(1994)122<0927:TSMECM>2.0.CO;2.

Janjić, Z.I., 1996. The surface layer in the NCEP Eta Model. In: 11th Conference on Numerical Weather Prediction. Amer Meteor Soc, Boston, MA, Norfolk, VA, pp. 354–355.

Janjić, Z.I., 2002. Nonsingular implementation of the Mellor-Yamada Level 2.5 Scheme in the NCEP Meso model.

Jordanov, G., Beezley, J.D., Dobrinkova, N., Kochanski, A.K., Mandel, J., Sousedík, B., 2012. Simulation of the 2009 Harmanli Fire (Bulgaria). In: Lecture Notes in Computer Science (Including Subseries Lecture Notes in Artificial Intelligence and Lecture Notes in Bioinformatics), pp. 291–298. https://doi.org/10.1007/978-3-642-29843-1_33.

José, R.S., Pérez, J.L., González, R.M., Pecci, J., Palacios, M., 2014. Analysis of fire behaviour simulations over Spain with WRF-FIRE. Int. J. Environ. Pollut. 55. https://doi.org/10.1504/IJEP.2014.065919.

Josipa, M., Joachim, I., Kirsten, W.-S., 2014. Soil texture forcing data for the whole world for the Weather Research and Forecasting (WRF) Model of the University of Hohenheim (UHOH) based on the Harmonized World Soil Database (HWSD) at 30 arc-second horizontal resolution. World Data Center for Clima.

Kalabokidis, K., Iliopoulos, N., Gliglinos, D., 2012. Pyro-Meteorology and wildfires behavior in an enviroment under change. IWN, Athens.

Karacostas, T., 2003. Synoptic, dynamic and cloud microphysical characteristics related to precipitation enhancement projects. In: Regional Seminar on Cloud Physics and Weather Modification. World Meteorological Organization, WMP No. 42. WMO-TD, pp. 194–200.

Karacostas, T., Flocas, A.A., Flocas, H.A., Kakaliagou, O., Rizou, C., 1992. A study of the

synoptic situations over the area of Eastern Mediterranean. 1st Greek Conference on Meteorology-Climatology-Physics of the Atmosphere. Thessaloniki, Greece.

Karacostas, T., Kartsios, S., Pytharoulis, I., Tegoulias, I., Bampzelis, D., 2018. Observations and modelling of the characteristics of convective activity related to a potential rain enhancement program in Central Greece. Atmos. Res. 208, 218–228. https://doi.org/10.1016/j.atmosres.2017.08.014.

Kartsios, S., Karacostas, T., Pytharoulis, I., Dimitrakopoulos, A.P., 2014a. Coupled Weather – Wildland Fire Model for fire behaviour interpretation. In: 12th International Conference on Meteorology, Climatology and Atmospheric Physics. COMECAP, Herakleion, Greece.

Kartsios, S., Karacostas, T., Pytharoulis, I., Dimitrakopoulos, A.P., 2014b. Simulating Atmosphere-Fire Interactions using a Coupled Weather – Wildland Fire Model. In: 10th Congress of the Hellenic Geographical Society. HGS, Thessaloniki, Greece.

Kartsios, S., Karacostas, T.S., Pytharoulis, I., Dimitrakopoulos, A.P., 2017. The Role of Heat Extinction Depth Concept to Fire Behavior: An Application to WRF-SFIRE Model. In: Karacostas, T., Bais, A., Nastos, P.T. (Eds.), Perspectives on Atmospheric Sciences. Springer International Publishing, Cham, pp. 137–142. https://doi.org/10.1007/978-3-319-35095-0_20.

Keeley, J.E., Fotheringham, C.J., 2001. History and Management of Crown-Fire Ecosystems: a Summary and Response. Conserv. Biol. 15, 1561–1567. https://doi.org/10.1046/j.1523-1739.2001.t01-1-00186.x.

Klein Tank, A.M.G., Wijngaard, J.B., Können, G.P., Böhm, R., Demarée, G., Gocheva, A., Mileta, M., Pashiardis, S., Hejkrlik, L., Kern-Hansen, C., Heino, R., Bessemoulin, P., Müller-Westermeier, G., Tzanakou, M., Szalai, S., Pálsdóttir, T., Fitzgerald, D., Rubin, S., Capaldo, M., Maugeri, M., Leitass, A., Bukantis, A., Aberfeld, R., van Engelen, A.F.V., Forland, E., Mietus, M., Coelho, F., Mares, C., Razuvaev, V., Nieplova, E., Cegnar, T., Antonio López, J., Dahlström, B., Moberg, A., Kirchhofer, W., Ceylan, A., Pachaliuk, O., Alexander, L.V., Petrovic, P., 2002. Daily dataset of 20th-century surface air temperature and precipitation series for the European Climate Assessment. Int. J. Climatol. 22, 1441–1453. https://doi.org/10.1002/joc.773.

Klemp, J.B., Durran, D.R., 1987. Numerical modelling of Bora winds. Meteorol. Atmos. Phys. 36, 215–227. https://doi.org/10.1007/BF01045150.

Klemp, J.B., Lilly, D.R., 1975. The Dynamics of Wave-Induced Downslope Winds. J. Atmos. Sci. 32, 320–339. https://doi.org/10.1175/1520-0469(1975)032<0320:TDOWID>2.0.CO;2.

Knorr, W., Pytharoulis, I., Petropoulos, G.P., Gobron, N., 2011. Combined use of weather forecasting and satellite remote sensing information for fire risk , fire and fire impact monitoring. Comput. Ecol. Softw. 1, 112–120.

Kochanski, A.K., Jenkins, M.A., Mandel, J., Beezley, J.D., Clements, C.B., Krueger, S., 2013a. Evaluation of WRF-SFIRE performance with field observations from the FireFlux experiment. Geosci. Model Dev. 6, 1109–1126. https://doi.org/10.5194/gmd-6-1109-2013.

Kochanski, A.K., Jenkins, M.A., Mandel, J., Beezley, J.D., Krueger, S.K., 2013b. Real time simulation of 2007 Santa Ana fires. For. Ecol. Manag. 294, 136–149. https://doi.org/10.1016/j.foreco.2012.12.014.

Kochanski, A.K., Jenkins, M.A., Sun, R., Krueger, S., Abedi, S., Charney, J., 2013c. The importance of low-level environmental vertical wind shear to wildfire propagation: Proof of concept. J. Geophys. Res. Atmos. 118, 8238–8252. https://doi.org/10.1002/jgrd.50436.

Kochanski, A.K., Jenkins, M.A., Yedinak, K., Mandel, J., Beezley, J., Lamb, B., 2016. Toward an integrated system for fire, smoke and air quality simulations. Int. J. Wildl. Fire 25, 534. https://doi.org/10.1071/WF14074.

Koletsis, I., Lagouvardos, K., Kotroni, V., Bartzokas, A., 2009. Numerical study of a downslope windstorm in Northwestern Greece. Atmos. Res. 94, 178–193. https://doi.org/10.1016/j.atmosres.2009.05.012.

Koletsis, I., Giannaros, T.M., Lagouvardos, K., Kotroni, V., 2016. Observational and numerical study of the Vardaris wind regime in northern Greece. Atmos. Res. 171, 107–120. https://doi.org/10.1016/j.atmosres.2015.12.011.

Kotroni, V., Lagouvardos, K., 2004. Evaluation of MM5 High-Resolution Real-Time Forecasts over the Urban Area of Athens. Greece. J. Appl. Meteorol. 43, 1666–1678. https://doi.org/10.1175/jam2170.1.

Kotroni, V., Lagouvardos, K., Lykoudis, S., 2014. High-resolution model-based wind atlas for Greece. Renew. Sust. Energ. Rev. 30, 479–489. https://doi.org/10.1016/J.RSER.2013.10.016.

Koutsias, N., Arianoutsou, M., Kallimanis, A.S., Mallinis, G., Halley, J.M., Dimopoulos, P., 2012. Where did the fires burn in Peloponnisos, Greece the summer of 2007? Evidence for a synergy of fuel and weather. Agric. For. Meteorol. 156, 41–53. https://doi.org/10.1016/j.agrformet.2011.12.006.

Krestenitis, Y., Pytharoulis, I., Karacostas, T.S., Androulidakis, Y., Makris, C., Kombiadou, K., Tegoulias, I., Baltikas, V., Kotsopoulos, S., Kartsios, S., 2017. Severe Weather Events and Sea Level Variability over the Mediterranean Sea: The WaveForUs Operational Platform. Springer, Cham, pp. 63–68. https://doi.org/10.1007/978-3-319-35095-0_9.

Lagouvardos, K., Kotroni, V., Defer, E., Bousquet, O., 2013. Study of a heavy precipitation event over southern France, in the frame of HYMEX project: Observational analysis and model results using assimilation of lightning. Atmos. Res. 134, 45–55. https://doi.org/10.1016/j.atmosres.2013.07.003.

Lagouvardos, K., Kotroni, V., Giannaros, T.M., Dafis, S., 2019. Meteorological Conditions Conducive to the Rapid Spread of the Deadly Wildfire in Eastern Attica, Greece. Bull. Am. Meteorol. Soc. 100, 2137–2145. https://doi.org/10.1175/BAMS-D-18-0231.1.

Lekkas, E., Carydis, P., Lagouvardos, K., Mavroulis, S., Diakakis, M., Andreadakis, E., Gogou, M.E., Spyrou, N.I., Athanassiou, M., Kapourani, E., Arianoutsou, M., Vassilakis, M., Kotsi, E., Speis, P.D., Delakouridis, J., Milios, D., Kotroni, V., Giannaros, T.M., Dafis, S., Karagiannidis, A., Papagiannaki, K., 2018. The July 2018 Attica (central Greece) wildfires - Scientific Report (Version 1.0) Newsletter of Environmental, Disaster, and Crisis Management Strategies (No. 8.). National and Kapodistrian University of Athens, Athens, Greece.

Li, J., Heap, A.D., 2014. Spatial interpolation methods applied in the environmental sciences: A review. Environ. Model. Softw. 53, 173–189. https://doi.org/10.1016/j.envsoft.2013.12.008.

Long, R.R., 1953. Some Aspects of the Flow of Stratified Fluids: I. A Theoretical Investigation. Tellus 5, 42–58. https://doi.org/10.3402/tellusa.v5i1.8563.

Long, R.R., 1955. Some Aspects of the Flow of Stratified Fluids: III. Continuous Density Gradients. Tellus 7, 341–357. https://doi.org/10.1111/j.2153-3490.1955.tb01171.x.

Mandel, J., Beezley, J.D., Kochanski, A.K., 2011. Coupled atmosphere-wildland fire modeling with WRF 3.3 and SFIRE 2011. Geosci. Model Dev. 4, 591–610. https://doi.org/10.5194/gmd-4-591-2011.

Mandel, J., Amram, S., Beezley, J.D., Kelman, G., Kochanski, A.K., Kondratenko, V.Y., Lynn, B.H., Regev, B., Vejmelka, M., 2014. Recent advances and applications of WRF-SFIRE. Nat. Hazards Earth Syst. Sci. 14, 2829–2845. https://doi.org/10.5194/nhess-14-2829-2014.

Matsangouras, I.T., Pytharoulis, I., Nastos, P.T., 2014. Numerical modeling and analysis of the effect of complex Greek topography on tornadogenesis. Hazards Earth Syst. Sci 14, 1905–1919. https://doi.org/10.5194/nhess-14-1905-2014.

Matsangouras, I.T., Nastos, P.T., Pytharoulis, I., 2016. Study of the tornado event in Greece on March 25, 2009: Synoptic analysis and numerical modeling using modified topography. Atmos. Res. 169, 566–583. https://doi.org/10.1016/j.atmosres.2015.08.010.

Minnich, R.A., 2001. An Integrated Model of Two Fire Regimes. Conserv. Biol. 15, 1549–1553. https://doi.org/10.1046/j.1523-1739.2001.01067.x.

Monin, A.S., Obukhov, A.M., 1954. Basic laws of turbulent mixing in the atmosphere near the ground. Tr. Akad. Nauk SSSR Geofiz. Inst 24, 163–187.

Moriondo, M., Good, P., Durao, R., Bindi, M., Giannakopoulos, C., Corte-Real, J., 2006. Potential impact of climate change on fire risk in the Mediterranean area. Clim. Res. 31, 85–95. https://doi.org/10.3354/cr031085.

Morvan, D., 2011. Physical Phenomena and Length Scales Governing the Behaviour of Wildfires: A Case for Physical Modelling. Fire. Technol 47, 437–460. https://doi.org/10.1007/s10694-010-0160-2.

Mukherjee, S., Schalkwijk, J., Jonker, H.J.J., Mukherjee, S., Schalkwijk, J., Jonker, H.J.J., 2016. Predictability of Dry Convective Boundary Layers: A LES Study. J. Atmos. Sci. 73, 2715–2727. https://doi.org/10.1175/JAS-D-15-0206.1.

NASA, 2013. NASA Shuttle Radar Topography Mission Global 1 arc second. NASA, JPL.

Nauslar, N., Abatzoglou, J., Marsh, P., 2018. The 2017 North Bay and Southern California Fires: A case study. Fire 1, 18. https://doi.org/10.3390/fire1010018.

Papadopoulos, A., Katsafados, P., 2009. Verification of operational weather forecasts from the POSEIDON system across the Eastern Mediterranean. Nat. Hazards Earth Syst. Sci. 9, 1299–1306. https://doi.org/10.5194/nhess-9-1299-2009.

Peace, M., Mattner, T., Mills, G., Kepert, J., McCaw, L., 2016. Coupled fire-atmosphere simulations of the Rocky River fire using WRF-SFIRE. J. Appl. Meteorol. Climatol. 55, 1151–1168. https://doi.org/10.1175/JAMC-D-15-0157.1.

Peltier, W.R., Clark, T.L., 1979. The evolution and stability of finite-amplitude mountain waves. Part II: surface wave drag and severe downslope windstorms. J. Atmos. Sci. 36, 1498–1529. https://doi.org/10.1175/1520-0469(1979)036<1498:TEASOF>2.0.CO;2.

Pereira, M.G., Trigo, R.M., da Camara, C.C., Pereira, J.M.C., Leite, S.M., 2005. Synoptic patterns associated with large summer forest fires in Portugal. Agric. For. Meteorol. 129, 11–25. https://doi.org/10.1016/J.AGRFORMET.2004.12.007.

Powers, J.G., Klemp, J.B., Skamarock, W.C., Davis, C.A., Dudhia, J., Gill, D.O., Coen, J.L., Gochis, D.J., Ahmadov, R., Peckham, S.E., Grell, G.A., Michalakes, J., Trahan, S., Benjamin, S.G., Alexander, C.R., Dimego, G.J., Wang, W., Schwartz, C.S., Romine, G.S., Liu, Z., Snyder, C., Chen, F., Barlage, M.J., Yu, W., Duda, M.G., 2017. The weather research and forecasting model: Overview, system efforts, and future directions. Bull. Am. Meteorol. Soc. 98, 1717–1737. https://doi.org/10.1175/BAMS-D-15-00308.1.

Prein, A.F., Gobiet, A., 2017. Impacts of uncertainties in European gridded precipitation observations on regional climate analysis. Int. J. Climatol. 37, 305–327. https://doi.org/10.1002/joc.4706.

Pytharoulis, I., 2018. Analysis of a Mediterranean tropical-like cyclone and its sensitivity to the sea surface temperatures. Atmos. Res. 208, 167–179. https://doi.org/10.1016/j.atmosres.2017.08.009.

Pytharoulis, I., Tegoulias, I., Kotsopoulos, S., Bampzelis, D., Karacostas, T., Katragkou, E., 2015. Verification of the operational high-resolution WRF forecasts produced by WaveForUs project. In: 16th Annual WRF Users' Workshop.

Pytharoulis, I., Kotsopoulos, S., Tegoulias, I., Kartsios, S., Bampzelis, D., Karacostas, T., 2016. Numerical modeling of an intense precipitation event and its associated lightning activity over northern Greece. Atmos. Res. 169, 523–538. https://doi.org/10.1016/j.atmosres.2015.06.019.

Pytharoulis, I., Kartsios, S., Tegoulias, I., Feidas, H., Miglietta, M., Matsangouras, I., Karacostas, T., 2018. Sensitivity of a Mediterranean tropical-like cyclone to physical parameterizations. Atmosphere (Basel). 9, 436. https://doi.org/10.3390/atmos9110436.

Rauthe, M., Steiner, H., Riediger, U., Mazurkiewicz, A., Gratzki, A., 2013. A Central European precipitation climatology – Part I: Generation and validation of a high-resolution gridded daily data set (HYRAS). Meteorol. Zeitschrift 22, 235–256. https://doi.org/10.1127/0941-2948/2013/0436.

Roads, J.O., Ueyoshi, K., Chen, S.C., Alpert, J., Fujioka, F., 1991. Medium-range fire weather forecasts. Int. J. Wildl. Fire 1, 159–176. https://doi.org/10.1071/WF9910159.

Rogers, E., Black, T., Ferrier, B., Lin, Y., Parrish, D., DiMego, G., 2001. Changes to the NCEP Meso Eta Analysis and Forecast System: Increase in Resolution, New Cloud Microphysics, Modified Precipitation Assimilation, Modified 3DVAR Analysis. NOAA/NWS Technical Procedures Bulletin 488, Washington, DC, USA.

Rothermel, R.C., 1972. A mathematical model for predicting fire spread in wildland fuels. Research Paper INT-116 USA. USDA Forest Service, Intermountain Forest and Range Experiment Station, Ogden, Utah 84401.

Rothermel, R.C., 1993. Mann Gulch Fire: A Race That Couldn't Be Won. General Technical Report INT-299 USDA Forest Service, Intermountain Research Station, Ogden, Utah 84401.

Sá, A.C.L., Benali, A., Fernandes, P.M., Pinto, R.M.S., Trigo, R.M., Salis, M., Russo, A., Jerez, S., Soares, P.M.M., Schroeder, W., Pereira, J.M.C., 2017. Evaluating fire growth simulations using satellite active fire data. Remote Sens. Environ. 190, 302–317. https://doi.org/10.1016/j.rse.2016.12.023.

Schroeder, W., Oliva, P., Giglio, L., Csiszar, I.A., 2014. The New VIIRS 375m active fire detection data product: Algorithm description and initial assessment. Remote Sens. Environ. 143, 85–96. https://doi.org/10.1016/j.rse.2013.12.008.

Scorer, R.S., Klieforth, H., 1959. Theory of mountain waves of large amplitude. Q. J. R. Meteorol. Soc. 85, 131–143. https://doi.org/10.1002/qj.49708536406.

Scott, J.H., Burgan, R.E., 2005. Standard fire behavior fuel models: a comprehensive set for use with Rothermel's surface fire spread model. USDA For. Serv. Gen. Tech. Rep. RMRS-GTR. https://doi.org/10.2737/RMRS-GTR-153.

Sebastián López, A., San-Miguel-Ayanz, J., Burgan, R.E., 2002. Integration of satellite sensor data, fuel type maps and meteorological observations for evaluation of forest fire risk at the pan-European scale. Int. J. Remote Sens. 23, 2713–2719. https://doi.org/10.1080/01431160110107761.

Sharples, J.J., 2009. An overview of mountain meteorological effects relevant to fire behaviour and bushfire risk. Int. J. Wildl. Fire 18, 737. https://doi.org/10.1071/WF08041.

Sharples, J.J., Mills, G.A., McRae, R.H.D., Weber, R.O., 2010. Foehn-Like Winds and Elevated Fire Danger Conditions in Southeastern Australia. J. Appl. Meteorol. Climatol. 49, 1067–1095. https://doi.org/10.1175/2010JAMC2219.1.

Sharples, J.J., McRae, R.H.D., Wilkes, S.R., 2012. Wind - terrain effects on the propagation of wildfires in rugged terrain: fire channelling. Int. J. Wildl. Fire 21, 282. https://doi.org/10.1071/WF10055.

Simpson, C.C., Sharples, J.J., Evans, J.P., 2014. Resolving vorticity-driven lateral fire spread using the WRF-Fire coupled atmosphere&ndash;fire numerical model. Nat. Hazards Earth Syst. Sci. 14, 2359–2371. https://doi.org/10.5194/nhess-14-2359-2014.

Simpson, C.C., Sharples, J.J., Evans, J.P., 2016. Sensitivity of atypical lateral fire spread to wind and slope. Geophys. Res. Lett. 43, 1744–1751. https://doi.org/10.1002/2015GL067343.

Simpson, C.C., Sharples, J.J., Evans, J.P., McCabe, M.F., 2013a. Large eddy simulation of atypical wildland fire spread on leeward slopes. Int. J. Wildl. Fire 22, 599. https://doi.org/10.1071/WF12072.

Simpson, C.C., Sturman, A., Zawar-Reza, P., Pearce, G., 2013b. Assessment of Fire Weather during a Foehn Event in South Island, New Zealand. In: 10th Bushfire CRC and 20th AFAC Conference conference. Bushfire CRC, Melbourne, Australia.

Sindosi, O.A., Bartzokas, A., Kotroni, V., Lagouvardos, K., 2012. Verification of precipitation forecasts of MM5 model over Epirus, NW Greece, for various convective parameterization schemes. Nat. Hazards Earth Syst. Sci. 12, 1393–1405. https://doi.org/10.5194/nhess-12-1393-2012.

Smith, R.B., 1985. On Severe Downslope Winds. J. Atmos. Sci. 42, 2597–2603. https://doi.org/10.1175/1520-0469(1985)042<2597:OSDW>2.0.CO;2.

Smolarkiewicz, P.K., Rotunno, R., 1989. Low froude number flow past three-dimensional obstacles. Part I: baroclinically generated lee Vortices. J. Atmos. Sci. 46, 1154–1164. https://doi.org/10.1175/1520-0469(1989)046<1154:LFNFPT>2.0.CO;2.

Stull, R., 1994. An Introduction to Boundary Layer Meteorology. Kluwer Academic Publishers, Dordrecht. https://doi.org/10.1007/978-94-009-3027-8.

Sun, W.-Y., 2013. Numerical study of severe downslope windstorm. Weather Clim. Extrem. 2, 22–30. https://doi.org/10.1016/j.wace.2013.10.002.

Tewari, M., Chen, F., Wang, W., Dudhia, J., Lemone, M.A., Mitchell, K., Ek, M., Gayno, G., Wegiel, J., Cuenca, R.H., 2004. Implementation and verification of the unified NOAH land surface model in the WRF model. In: 20th Conference on Weather Analysis and Forecasting/16th Conference on Numerical Weather Prediction, pp. 11–15.

Tolika, K., Maheras, P., Tegoulias, I., 2009. Extreme temperatures in Greece during 2007: Could this be a "return to the future"? Geophys. Res. Lett. 36, L10813. https://doi.org/10.1029/2009GL038538.

Ulmer, F.-G., Balss, U., 2016. Spin-up time research on the weather research and forecasting model for atmospheric delay mitigations of electromagnetic waves. J. Appl. Rem. Sens. 10, 016027. https://doi.org/10.1117/1.JRS.10.016027.

Vázquez, A., Pérez, B., Fernández-González, F., Moreno, J.M., 2002. Recent fire regime characteristics and potential natural vegetation relationships in Spain. J. Veg. Sci. 13, 663–676. https://doi.org/10.1111/j.1654-1103.2002.tb02094.x.

Viegas, D.X., 2009. Recent forest fire related accidents in Europe. Ispra. https://doi.org/10.2788/50781.

Wang, W., Bruyère, C., Duda, M.G., Dudhia, J., Gill, D.O., Hin, H.C., Michalakes, J., Rizvi, S., Zhang, X., Beezley, J.D., Coen, J.L., Mandel, J., Chuang, H.-Y., Mckee, N., Slovacek, T., Wolff, J., 2012. ARW Version 3 Modeling System User's Guide.

Weiss, S.J., Pyle, M.E., Janjic, Z., Bright, D.R., Kain, J.S., Dimego, G.J., 2008. The Operational High Resolution Window WRF Model Runs at NCEP : Advantages of Multiple Model Runs for Severe Convective Weather Forecasting. In: 24th Conference on Severe Local Storms. American Meteorological Society, Savannah, GA.

Whiteman, C.D., 2000. Mountain Meteorology: Fundamentals and Applications. Oxford University Press, New York.

Yair, Y., Lynn, B., Price, C., Kotroni, V., Lagouvardos, K., Morin, E., Mugnai, A., Llasat, M., 2010. Predicting the potential for lightning activity in Mediterranean storms based on the Weather Research and Forecasting (WRF) model dynamic and microphysical fields. J. Geophys. Res. 115, D04205. https://doi.org/10.1029/2008JD010868.

Young, J.A., North, G.R., Pyle, J.A., Zhang, F., 2003. Static stability. In: Encyclopedia of Atmospheric Sciences. vol. 1–6. Elsevier, pp. 2998.